Chapter 2
Finite Element Method on Polytopal Meshes

The finite element method (FEM) is a powerful tool for the approximation of boundary value problems, which is widely applied and accepted in science and engineering. The approach relies on the decomposition of the underlying domain into elements and the construction of a discrete approximation space over the given discretization. The BEM-based finite element method can be seen as a generalization in order to handle more general elements in the mesh. This chapter contains a discussion of polygonal as well as polyhedral meshes and the construction of basis functions for the approximation space over these general meshes. The formulation of the BEM-based FEM is obtained by means of a Galerkin formulation and its convergence and approximation properties are analysed with the help of introduced interpolation operators. Numerical experiments confirm the theoretical findings.

2.1 Preliminaries

The approximation space in the BEM-based finite element method is defined in accordance with the underlying differential equation of the considered boundary value problem. For this presentation, we choose the diffusion problem with mixed boundary conditions on a bounded polygonal/polyhedral domain $\Omega \subset \mathbb{R}^d, d = 2, 3$. Its boundary $\Gamma = \Gamma_D \cup \Gamma_N$ is split into a Dirichlet and a Neumann part, where we assume $|\Gamma_D| > 0$. Given a source term $f \in L_2(\Omega)$, a Dirichlet datum $g_D \in H^{1/2}(\Gamma_D)$ as well as a Neumann datum $g_N \in L_2(\Gamma_N)$, the problem reads

$$\begin{aligned} -\operatorname{div}(a\nabla u) &= f \quad && \text{in } \Omega\ , \\ u &= g_D \quad && \text{on } \Gamma_D\ , \\ a\nabla u \cdot \mathbf{n} &= g_N \quad && \text{on } \Gamma_N\ , \end{aligned} \tag{2.1}$$

S. Weißer, *BEM-based Finite Element Approaches on Polytopal Meshes*,
Lecture Notes in Computational Science and Engineering 130,
https://doi.org/10.1007/978-3-030-20961-2_2

where $a \in L_\infty(\Omega)$ with $0 < a_{\min} \leq a \leq a_{\max}$ almost everywhere in Ω and $\mathbf{n}$ is the outward unit normal vector on Γ. This boundary value problem is considered in the week sense with the help of a Galerkin formulation. Thus, we seek a solution $u \in H^1(\Omega)$, where we denote, as usual, the Sobolev spaces of order $s \in \mathbb{R}$ with $H^s(D)$ for some domain $D \subset \Omega$, cf. Sect. 1.3. Furthermore, we utilize the space of polynomials $\mathscr{P}^k(D)$ with degree smaller or equal $k \in \mathbb{N}_0$ with the convention that $\mathscr{P}^{-1}(D) = \{0\}$. Here, D might also be a one- or two-dimensional submanifold of Ω. For simplicity, we assume in the first part that the diffusion coefficient a is piecewise constant and its jumps are resolved by the meshes later on. Nevertheless, we will also give a strategy for the more general situation of continuously varying diffusion coefficients. Our goal is to introduce a H^1-conforming approximation space of arbitrary order $k \in \mathbb{N}$ which yields optimal rates of convergence in the finite element framework. In all estimates, c denotes a generic constant that depends on the mesh regularity and stability, the space dimension d and the approximation order k. The following discrete approximation of $H^1(\Omega)$ is constructed but not limited to the diffusion equation. It can also be applied to other boundary value problems where H^1-conforming approximations are desirable.

2.2 Polygonal and Polyhedral Meshes

For the finite element method, we have to introduce a discretization $\mathscr{K}_h$ of Ω. In this section, we distinguish the two- and three-dimensional case $\Omega \subset \mathbb{R}^d$, $d = 2, 3$. In contrast to classical conforming finite element methods, we allow meshes with general polygonal and polyhedral elements which are bounded. Examples of such meshes are given in Fig. 2.1. If we do not distinguish between the space dimension d, we call the meshes and the elements polytopal. The elements $K \in \mathscr{K}_h$

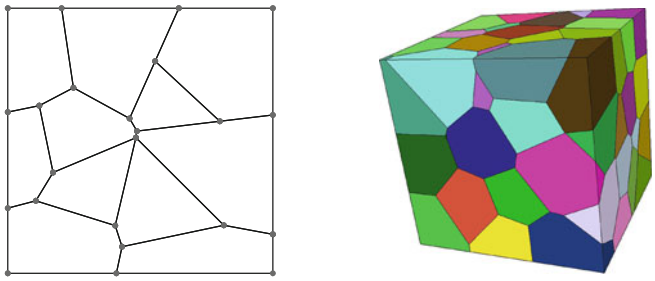

Fig. 2.1 Two examples for meshes with polygonal and polyhedral elements

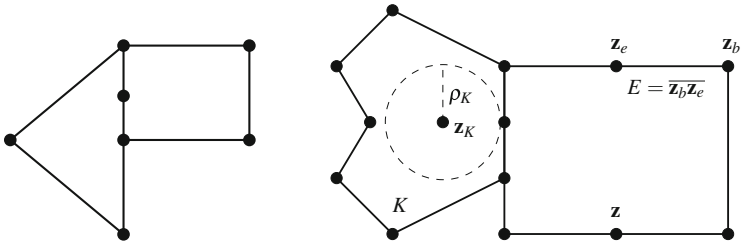

Fig. 2.2 Two examples of neighbouring elements with additional nodes on the straight boundary

are non-overlapping open sets such that

$$\overline{\Omega} = \bigcup_{K \in \mathscr{K}_h} \overline{K} \, .$$

The boundaries of the elements consist of nodes and edges in 2D as well as of faces in 3D. An edge $E = \overline{\mathbf{z}_b\mathbf{z}_e}$ is always located between two nodes, the one at the beginning $\mathbf{z}_b$ and the one at the end $\mathbf{z}_e$. These points are fixed once per edge and they are the only nodes on E. In each corner of an element K, a node is located, but in 2D there could also be some nodes on straight lines of the polygonal boundary ∂K, cf. Fig. 2.2. We stress this fact more carefully. If we have a triangle with three nodes and we add some nodes on the boundary, this triangle turns formally into a polygon. These additional nodes enrich the approximation space in the finite element method. In this context, nodes on straight lines are natural since they are just ordinary nodes for polygons. In triangular or quadrilateral meshes these nodes appear as hanging nodes which are undesirable and do not influence the accuracy of the approximation. In classical finite element implementations, such hanging nodes have to be treated in a special way as conditional nodes or by removing them. Methods working on polygonal meshes include such nodes naturally. In 3D, hanging nodes appear naturally on edges of the polyhedral elements and one may have hanging edges on the polygonal faces. The polygonal faces are assumed to be flat and they are surrounded by edges which are coplanar.

For the later analysis, we need some notation. $\mathscr{N}_h$ denotes the set of all nodes in the mesh $\mathscr{K}_h$. It is $\mathscr{N}_h = \mathscr{N}_{h,\Omega} \cup \mathscr{N}_{h,D} \cup \mathscr{N}_{h,N}$, where $\mathscr{N}_{h,\Omega}$, $\mathscr{N}_{h,D}$, $\mathscr{N}_{h,N}$ contain the nodes in the interior of Ω, on the Dirichlet boundary Γ_D and on the interior of the Neumann boundary Γ_N, respectively. The transition points between Γ_D and Γ_N belong to $\mathscr{N}_{h,D}$. We denote the set of all edges of the mesh with $\mathscr{E}_h$. In analogy to the set of nodes, we decompose $\mathscr{E}_h = \mathscr{E}_{h,\Omega} \cup \mathscr{E}_{h,D} \cup \mathscr{E}_{h,N}$, where $\mathscr{E}_{h,\Omega}$, $\mathscr{E}_{h,D}$ and $\mathscr{E}_{h,N}$ contain all edges in the interior of Ω, on the Dirichlet boundary Γ_D and on the Neumann boundary Γ_N, respectively. In 3D, we additionally have the set of all faces $\mathscr{F}_h = \mathscr{F}_{h,\Omega} \cup \mathscr{F}_{h,D} \cup \mathscr{F}_{h,N}$ with subsets analogous as before. Moreover, the sets $\mathscr{N}(K)$, $\mathscr{N}(E)$ and $\mathscr{N}(F)$ contain all nodes which belong to the element $K \in \mathscr{K}_h$, the edge $E \in \mathscr{E}_h$ and the face $F \in \mathscr{F}_h$, respectively. We denote the set of edges which belong to the element K by $\mathscr{E}(K)$ and those which belong to a face F

by $\mathscr{E}(F)$. The set $\mathscr{F}(K)$ contains finally the faces of an element K. The union of the boundaries of all elements

$$\Gamma_S = \bigcup_{K \in \mathscr{K}_h} \partial K$$

is said to be the skeleton of the discretization.

2.2.1 Mesh Regularity and Properties in 2D

The length of an edge E and the diameter of an element K are denoted by h_E and $h_K = \sup\{|x - y| : x, y \in \partial K\}$, respectively.

Definition 2.1 (Regular Mesh in 2D) The family of meshes $\mathscr{K}_h$ is called regular if it satisfies:

1. Each element $K \in \mathscr{K}_h$ is a star-shaped polygon with respect to a circle of radius ρ_K and midpoint $\mathbf{z}_K$.
2. The aspect ratio is uniformly bounded from above by $\sigma_{\mathscr{K}}$, i.e. $h_K/\rho_K < \sigma_{\mathscr{K}}$ for all $K \in \mathscr{K}_h$.

The circle in the definition is chosen in such a way that its radius is maximal, cf. Fig. 2.2. If the position of the circle is not unique, its midpoint $\mathbf{z}_K$ is fixed once per element. Additionally, we assume that $h_K < 1$ for all elements $K \in \mathscr{K}_h$. This condition is no grievous restriction on the mesh since $h_K < 1$ can always be satisfied by scaling Ω. Nevertheless, it is necessary in the forthcoming local boundary integral formulations in 2D.

For the analysis of local boundary element methods used in the BEM-based FEM and some proofs in Chap. 5, the regularity of a mesh is not enough. Another important property is that the diameter of an element is comparable to the length of its shortest edge. This is ensured by the following definition.

Definition 2.2 (Stable Mesh in 2D) The family of meshes $\mathscr{K}_h$ is called stable if there is a constant $c_{\mathscr{K}} > 0$ such that for all elements $K \in \mathscr{K}_h$ and all its edges $E \in \mathscr{E}(K)$ it holds

$$h_K \leq c_{\mathscr{K}} h_E.$$

When we consider convergence or error estimates with respect to the mesh size $h = \max\{h_K : K \in \mathscr{K}_h\}$, it is important that the constants in the definitions above hold uniformly for the whole family of meshes. For convenience we only write mesh and mean a whole family for $h \to 0$.

In the following, we give some useful properties of regular meshes. An important analytical tool is an auxiliary triangulation $\mathscr{T}_h(K)$ of the elements $K \in \mathscr{K}_h$. This triangulation is constructed by connecting the nodes on the boundary of K with

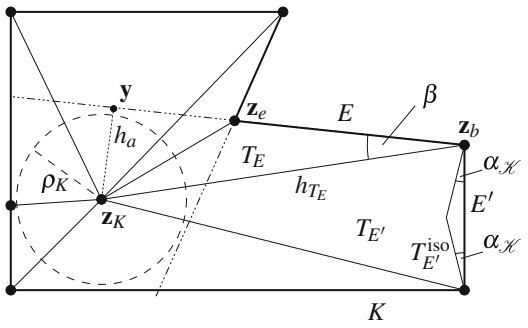

Fig. 2.3 Auxiliary triangulation $\mathscr{T}_h(K)$ of star-shaped element K, altitude $h_a = \mathrm{alt}(T_E, E)$ of triangle $T_E \in \mathscr{T}_h(K)$ perpendicular to E and angle $\beta = \angle \mathbf{z}_K \mathbf{z}_b \mathbf{z}_e$ as well as triangle $T_{E'} \in \mathscr{T}_h(K)$ with isosceles triangle $T_{E'}^{\mathrm{iso}}$

the point $\mathbf{z}_K$ of Definition 2.1, see Fig. 2.3. Consequently, $\mathscr{T}_h(K)$ consists of the triangles T_E for $E = \overline{\mathbf{z}_b \mathbf{z}_e} \in \mathscr{E}(K)$, which are defined by the points $\mathbf{z}_b$, $\mathbf{z}_e$ and $\mathbf{z}_K$.

Lemma 2.3 *Let K be a polygonal element of a regular and stable mesh $\mathscr{K}_h$. The auxiliary triangulation $\mathscr{T}_h(K)$ is shape-regular in the sense of Ciarlet [58], i.e., neighbouring triangles share either a common node or edge and the aspect ratio of each triangle is uniformly bounded by some constant $\sigma_{\mathscr{T}}$, which only depends on $\sigma_{\mathscr{K}}$ and $c_{\mathscr{K}}$.*

Proof Let $T_E \in \mathscr{T}_h(K)$ be a triangle with diameter h_{T_E} and let ρ_{T_E} be the radius of the incircle. It is known that the area of T_E is given by $|T_E| = \frac{1}{2}|\partial T_E| \rho_{T_E}$, where $|\partial T_E|$ is the perimeter of T_E. Obviously, it is $|\partial T_E| \leq 3 h_{T_E}$. On the other hand, we have the formula $|T_E| = \frac{1}{2} h_E h_a$, where $h_a = \mathrm{alt}(T_E, E)$ is the altitude of the triangle perpendicular to E, see Fig. 2.3. Since the element K is star-shaped with respect to a circle of radius ρ_K, the line through the side $E \in \mathscr{E}_h$ of the triangle does not intersect this circle. Thus, $h_a \geq \rho_K$ and we have the estimate $|T_E| \geq \frac{1}{2} h_E \rho_K$. Together with Definition 2.1, we obtain

$$\frac{h_{T_E}}{\rho_{T_E}} = \frac{|\partial T_E| h_{T_E}}{2|T_E|} \leq \frac{3 h_{T_E}^2}{h_E \rho_K} \leq 3 c_{\mathscr{K}} \sigma_{\mathscr{K}} \frac{h_{T_E}^2}{h_K^2} \leq 3 c_{\mathscr{K}} \sigma_{\mathscr{K}} = \sigma_{\mathscr{T}} \, .$$

□

In the previous proof, we discovered and applied the estimate

$$|T_E| \geq \tfrac{1}{2} h_E \rho_K \tag{2.2}$$

for the area of the auxiliary triangle. This inequality will be of importance once more. We may also consider the auxiliary triangulation $\mathscr{T}_h(\mathscr{K}_h)$ of the whole domain Ω which is constructed by gluing the local triangulations $\mathscr{T}_h(K)$. Obviously, $\mathscr{T}_h(\mathscr{K}_h)$ is also shape-regular in the sense of Ciarlet. Furthermore, the angles in the auxiliary triangulation $\mathscr{T}_h(K)$ next to ∂K can be bounded from below. This gives rise to the following result.

Lemma 2.4 *Let $\mathscr{K}_h$ be a regular polygonal mesh. There is an angle $\alpha_{\mathscr{K}}$ with $0 < \alpha_{\mathscr{K}} \leq \pi/3$ such that for all elements $K \in \mathscr{K}_h$ and all its edges $E \in \mathscr{E}(K)$ the isosceles triangle T_E^{iso} with longest side E and two interior angles $\alpha_{\mathscr{K}}$ lies inside $T_E \in \mathscr{T}_h(K)$ and thus inside the element K, see Fig. 2.3. The angle $\alpha_{\mathscr{K}}$ only depends on $\sigma_{\mathscr{K}}$.*

Proof Let $T_E \in \mathscr{T}_h(K)$. We bound the angle $\beta = \angle \mathbf{z}_K \mathbf{z}_b \mathbf{z}_e$ in T_E next to $E = \overline{\mathbf{z}_b \mathbf{z}_e}$ from below, see Fig. 2.3. Without loss of generality, we assume that $\beta < \pi/2$. Using the projection $\mathbf{y}$ of $\mathbf{z}_K$ onto the straight line through the edge E, we recognize

$$\sin\beta = \frac{|\mathbf{y} - \mathbf{z}_K|}{|\mathbf{z}_b - \mathbf{z}_K|} \geq \frac{\rho_K}{h_K} \geq \frac{1}{\sigma_{\mathscr{K}}} \in (0, 1) \,. \tag{2.3}$$

Consequently, it is $\beta \geq \arcsin \sigma_{\mathscr{K}}^{-1}$. Since this estimate is valid for all angles next to ∂K of the auxiliary triangulation, the isosceles triangles T_E^{iso}, $E \in \mathscr{E}(K)$ with common angle $\alpha_{\mathscr{K}} = \min\{\pi/3, \arcsin \sigma_{\mathscr{K}}^{-1}\}$ lie inside the auxiliary triangles T_E and therefore inside K. □

Remark 2.5 The upper bound of $\alpha_{\mathscr{K}}$ is chosen in such a way that the longest side of the isosceles triangle T_E^{iso} is always the edge E. This fact is not important in the previous lemma, but it simplifies forthcoming proofs.

Corollary 2.6 *Let $\mathscr{K}_h$ be a regular mesh. Every node belongs to a uniformly bounded number of elements, i.e. $|\{K \in \mathscr{K}_h : \mathbf{z} \in \mathscr{N}(K)\}| \leq c$, $\forall \mathbf{z} \in \mathscr{N}_h$. The constant $c > 0$ only depends on $\sigma_{\mathscr{K}}$.*

Proof Due to the regularity of $\mathscr{K}_h$, every interior angle of an element is bounded from below by $\alpha_{\mathscr{K}}$ as we have seen in Lemma 2.4. This angle only depends on $\sigma_{\mathscr{K}}$. Therefore, we have

$$|\{K \in \mathscr{K}_h : \mathbf{z} \in \mathscr{N}(K)\}| \leq \left\lfloor \frac{2\pi}{\alpha_{\mathscr{K}}} \right\rfloor \,,$$

where the term on the right hand side denotes the biggest integer smaller than or equal to $2\pi/\alpha_{\mathscr{K}}$. □

Conversely, we have a more restrictive result, which additionally assumes the stability of the mesh. Without the stability, the lengths of the edges might degenerate and thus a regular polygonal element can have arbitrary many nodes on its boundary.

Lemma 2.7 *Let $\mathscr{K}_h$ be regular and stable. Every element contains a uniformly bounded number of nodes and edges, i.e. $|\mathscr{N}(K)| = |\mathscr{E}(K)| \leq c$, $\forall K \in \mathscr{K}_h$. The constant $c > 0$ only depends on $\sigma_{\mathscr{K}}$ and $c_{\mathscr{K}}$.*

Proof We exploit the regularity of the mesh. Let $K \in \mathscr{K}_h$. In 2D it is obviously $|\mathscr{N}(K)| = |\mathscr{E}(K)|$. With the help of (2.2), we obtain

$$\begin{aligned} h_K^2 |\mathscr{N}(K)| &\leq \sigma_{\mathscr{K}} \rho_{\mathscr{K}} \, h_K |\mathscr{E}(K)| \\ &\leq \sigma_{\mathscr{K}} \rho_{\mathscr{K}} \sum_{E \in \mathscr{E}(K)} c_{\mathscr{K}} h_E \\ &\leq \sigma_{\mathscr{K}} c_{\mathscr{K}} \sum_{E \in \mathscr{E}(K)} 2|T_E| \\ &= 2\sigma_{\mathscr{K}} c_{\mathscr{K}} \, |K| \\ &\leq 2\sigma_{\mathscr{K}} c_{\mathscr{K}} \, h_K^2 \, . \end{aligned}$$

Consequently, we have $|\mathscr{N}(K)| \leq 2\sigma_{\mathscr{K}} c_{\mathscr{K}}$. □

The isosceles triangles and the auxiliary triangulation play an important role in the analysis of error estimates later on. They are used in order to handle polygonal elements and, in particular, to apply some results on interpolation of functions over triangulations. Such results are applicable, if the polygonal mesh is regular and stable, since then, the auxiliary triangulation is regular in the sense of Ciarlet according to Lemma 2.3. However, in certain situations, we can weaken the assumptions on the polygonal mesh and remove the stability. In [84], the following result is proven with similar considerations as in the proof of Lemma 2.4 for convex elements. However, the result is also valid in our more general case.

Lemma 2.8 *For a regular mesh $\mathscr{K}_h$, all angles of all triangles in the auxiliary triangulation $\mathscr{T}_h(\mathscr{K}_h)$ are less than $\pi - \arcsin \sigma_{\mathscr{K}}^{-1}$ and, in particular, they are strictly less than π.*

Proof We proceed similar as in the proof of Lemma 2.4. Therefore, let $K \in \mathscr{K}_h$ be an element with edge $E = \overline{\mathbf{z}_b \mathbf{z}_e}$ and we consider the triangle $T_E \in \mathscr{T}_h(K)$. It is sufficient to bound the angle $\angle \mathbf{z}_b \mathbf{z}_K \mathbf{z}_e$ and the larger angle of the others adjacent to E, lets say $\angle \mathbf{z}_b \mathbf{z}_e \mathbf{z}_K$. It is easily seen form (2.3) that

$$\angle \mathbf{z}_b \mathbf{z}_K \mathbf{z}_e \leq \pi - 2 \arcsin \sigma_{\mathscr{K}}^{-1} \, .$$

In order to bound $\angle \mathbf{z}_b \mathbf{z}_e \mathbf{z}_K$ we employ the point $\mathbf{y}$ once more which is the projection of $\mathbf{z}_K$ onto the line through E, see Fig. 2.3. Without loss of generality we assume $\angle \mathbf{z}_b \mathbf{z}_e \mathbf{z}_K > \pi/2$ and thus $\mathbf{y} \notin \overline{\mathbf{z}_b \mathbf{z}_e}$. It is

$$\sin(\pi - \angle \mathbf{z}_b \mathbf{z}_e \mathbf{z}_K) = \sin(\angle \mathbf{z}_K \mathbf{z}_e \mathbf{y}) = \frac{|\mathbf{y} - \mathbf{z}_K|}{|\mathbf{z}_e - \mathbf{z}_K|} \geq \frac{\rho_K}{h_K} \geq \frac{1}{\sigma_{\mathscr{K}}} \, .$$

Applying arcsin yields $\angle \mathbf{z}_b \mathbf{z}_e \mathbf{z}_K \leq \pi - \arcsin \sigma_{\mathscr{K}}^{-1}$ and the result follows because of $\arcsin \sigma_{\mathscr{K}}^{-1} > 0$ due to $\sigma_{\mathscr{K}} > 0$. □

An important consequence of this proposition is the following corollary.

Corollary 2.9 *Let $K \in \mathscr{K}_h$ be an element of a regular polygonal mesh $\mathscr{K}_h$. The auxiliary triangulations $\mathscr{T}_h(K)$ and $\mathscr{T}_h(\mathscr{K}_h)$ satisfy a maximum angle condition, i.e., every angle in the triangles of the mesh is uniformly bounded from above by a constant which is strictly less than π. The maximum angle only depends on $\sigma_{\mathscr{K}}$.*

Therefore, several approximation properties of finite element interpolation for linear as well as for higher order basis functions are valid on this auxiliary discretization, see [14, 114]. The constants appearing in those estimates depend on the maximum angle and thus, on the aspect ratio $\sigma_{\mathscr{K}}$ of the mesh $\mathscr{K}_h$, but not on the stability parameter $c_{\mathscr{K}}$.

2.2.2 Mesh Regularity and Properties in 3D

In addition to the diameter h_K of an element $K \in \mathscr{K}_h$ and the edge length h_E of $E \in \mathscr{E}_h$, we use the diameter h_F of polygonal faces $F \in \mathscr{F}_h$ in the following.

Definition 2.10 (Regular Faces) A set of faces $\mathscr{F}_h$ is called regular if all faces are flat polygons which are regular in the sense of Definition 2.1 with regularity parameter $\sigma_{\mathscr{F}}$. The radius of the inscribed circle of $F \in \mathscr{F}_h$ is denoted by ρ_F and its center by $\mathbf{z}_F$.

Definition 2.11 (Regular Mesh in 3D) The family of meshes $\mathscr{K}_h$ is called regular if it satisfies:

1. The associated set of faces $\mathscr{F}_h$ is regular.
2. Each element $K \in \mathscr{K}_h$ is a star-shaped polyhedron with respect to a ball of radius ρ_K and midpoint $\mathbf{z}_K$.
3. The aspect ratio is uniformly bounded from above by $\sigma_{\mathscr{K}}$, i.e. $h_K/\rho_K < \sigma_{\mathscr{K}}$ for all $K \in \mathscr{K}_h$.

The ball in the definition is chosen in such a way that its radius is maximal and, if its position is not unique, the midpoint $\mathbf{z}_K$ is fixed once per element. In contrast to the two-dimensional case, we do not impose the restriction on the diameter of the elements.

Definition 2.12 (Stable Mesh in 3D) The family of meshes $\mathscr{K}_h$ is called stable if there is a constant $c_{\mathscr{K}} > 0$ such that for all elements $K \in \mathscr{K}_h$ and all its edges $E \in \mathscr{E}(K)$ it holds

$$h_K \leq c_{\mathscr{K}} h_E.$$

When we consider convergence or error estimates with respect to the mesh size $h = \max\{h_K : K \in \mathscr{K}_h\}$, it is important that the constants in the definitions above hold uniformly for the whole family of meshes. As in the two-dimensional case, we only write mesh in the following and mean a whole family for $h \to 0$. The stability ensures that for an element the lengths of its edges, the diameters of its faces and

the diameter of itself are comparable. It yields

$$h_E \le h_F \le h_K \le c_{\mathscr{K}} h_E \le c_{\mathscr{K}} h_F$$

for $K \in \mathscr{K}_h$ and all $F \in \mathscr{F}(K)$ and $E \in \mathscr{E}(F)$.

Remark 2.13 For a regular and stable mesh $\mathscr{K}_h$, it holds

$$h_K^{d-1} \le c\,|F|\,, \tag{2.4}$$

for $K \in \mathscr{K}_h$ with $F \in \mathscr{F}(K)$. This is a direct generalization of the stability condition in two-dimensions, cf. Definition 2.2. Thus, (2.4) is valid for $d = 2, 3$ if F is interpreted as edge and face, respectively. This inequality follows by

$$|F| \ge \pi \rho_F^2 \ge \pi \frac{h_F^2}{\sigma_{\mathscr{F}}^2} \ge \pi \frac{h_K^2}{c_{\mathscr{K}}^2 \sigma_{\mathscr{F}}^2}\,.$$

In the derivation of interpolation and error estimates, an auxiliary discretization into tetrahedra will be the counterpart to the constructed triangulation in 2D. We employ the introduced auxiliary triangulation from Sect. 2.2.1 in order to discretize the polygonal faces and denote it by $\mathscr{T}_0(F)$ for $F \in \mathscr{F}_h$. Note, that we have chosen an index 0 instead of h. We introduce a family $\mathscr{T}_l(F)$ of triangulations, where the meshes of level $l \ge 1$ are defined recursively by splitting each triangle of the previous level into four similar triangles, see Fig. 2.4. The set of nodes in the triangular mesh is denoted by $\mathscr{M}_l(F)$. Obviously, the discretizations of the faces can be combined to a whole conforming surface mesh of an element $K \in \mathscr{K}_h$ by setting

$$\mathscr{T}_l(\partial K) = \bigcup_{F \in \mathscr{F}(K)} \mathscr{T}_l(F) \quad \text{and} \quad \mathscr{M}_l(\partial K) = \bigcup_{F \in \mathscr{F}(K)} \mathscr{M}_h(F)\,.$$

Finally, the auxiliary tetrahedral mesh $\mathscr{T}_l(K)$ of the polyhedral element $K \in \mathscr{K}_h$ is constructed by connecting the nodes of the triangular surface mesh $\mathscr{T}_l(\partial K)$ with

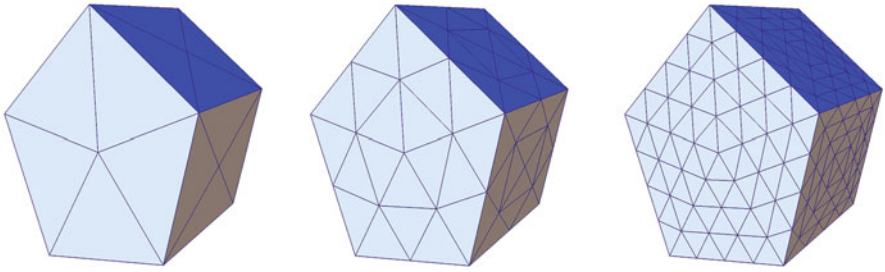

Fig. 2.4 Polyhedral element with surface triangulations of level $l = 0, 1, 2$

the point $\mathbf{z}_K$. The tetrahedra constructed this way are denoted by T_{tet}. Although, this auxiliary discretization may contain needle-like tetrahedra, their regularity can be controlled by the mesh regularity and stability of the polyhedral mesh. Combining the tetrahedral discretizations of the polyhedral elements forms an auxiliary discretization $\mathscr{T}_l(\mathscr{K}_h)$ for the whole domain Ω. If the mesh level l is not important in later proofs and $l = 0$ is sufficient, we also write $\mathscr{T}_h(\cdot)$ for $\mathscr{T}_0(\cdot)$ in order to treat the two- and three-dimensional cases simultaneously.

Lemma 2.14 *Let K be a polyhedral element of a regular and stable mesh $\mathscr{K}_h$. The auxiliary discretizations $\mathscr{T}_l(K)$ and $\mathscr{T}_l(\mathscr{K}_h)$, $l \geq 0$ are shape-regular in the sense of Ciarlet [58], i.e., neighbouring tetrahedra share either a common node, edge or triangular face and the aspect ratio of each tetrahedra is uniformly bounded by some constant $\sigma_{\mathscr{T}}$, which only depends on $\sigma_{\mathscr{K}}$, $\sigma_{\mathscr{F}}$, $c_{\mathscr{K}}$ and the mesh level l in the face discretization.*

Proof The conformity of the auxiliary mesh is rather obvious. Thus, we only have to bound the aspect ratio of the tetrahedra $T_{\text{tet}} \in \mathscr{T}_l(K)$, i.e., the ratio of the diameter $h_{T_{\text{tet}}}$ and the radius $\rho_{T_{\text{tet}}}$ of their insphere. For an arbitrary tetrahedron, we have the relation

$$\rho_{T_{\text{tet}}} = \frac{3V_{T_{\text{tet}}}}{A_{T_{\text{tet}}}} ,$$

where $V_{T_{\text{tet}}}$ is the volume and $A_{T_{\text{tet}}}$ is the surface area of the tetrahedron. This relation is seen as follows. $V_{T_{\text{tet}}}$ is equal to the sum of the volumes $V_{T_{\text{tet},i}}$, $i = 1, \ldots, 4$, of the four tetrahedra $T_{\text{tet},i}$ obtained by connecting the vertexes with the center of the insphere. Each volume is computed as $V_{T_{\text{tet},i}} = \frac{1}{3}\rho_{T_{\text{tet}}}|T_i|$, where T_i is the triangle on the surface of the initial tetrahedron T_{tet} and $\rho_{T_{\text{tet}}}$ corresponds to the hight of $T_{\text{tet},i}$ over T_i. Consequently, it holds

$$V_{T_{\text{tet}}} = \sum_{i=1}^{4} V_{T_{\text{tet},i}} = \sum_{i=1}^{4} \frac{1}{3}\rho_{T_{\text{tet}}}|T_i| = \frac{1}{3}\rho_{T_{\text{tet}}} A_{T_{\text{tet}}} .$$

First, we study the case $l = 0$, where only one node per face is added for the triangulation of the element surface. We consider the auxiliary discretization and choose an arbitrary tetrahedron T_{tet} with corresponding triangle $T \in \mathscr{T}_l(F)$ in some face $F \in \mathscr{F}(K)$ and with an edge $E \in \mathscr{E}(F)$ such that $E \subset \partial T \cap \partial F$. A rough estimate for the surface area of this tetrahedron is

$$A_{T_{\text{tet}}} = \sum_{i=1}^{4} |T_i| \leq \sum_{i=1}^{4} \frac{h_K^2}{2} = 2h_K^2 .$$

Let $\mathrm{alt}(T_{\mathrm{tet}}, T)$ be the altitude of the tetrahedron T_{tet} over the side T and let $\mathrm{alt}(T, E)$ be the altitude of the triangle T over the edge E. For the volume of T_{tet}, we have

$$V_{T_{\mathrm{tet}}} = \frac{1}{3}\,\mathrm{alt}(T_{\mathrm{tet}}, T)|T| = \frac{1}{6}\,\mathrm{alt}(T_{\mathrm{tet}}, T)\ \mathrm{alt}(T, E)\, h_E \ .$$

Since the faces of the element K and the element itself are star-shaped with respect to circles and a ball according to Definitions 2.10 and 2.11, it holds $\rho_F \leq \mathrm{alt}(T, E)$ as well as $\rho_K \leq \mathrm{alt}(T_{\mathrm{tet}}, T)$ due to the construction of T_{tet} and T. Consequently, we obtain

$$V_{T_{\mathrm{tet}}} \geq \frac{1}{6}\rho_K \rho_F h_E \geq \frac{1}{6\sigma_{\mathscr{K}}\sigma_{\mathscr{F}}} h_K h_F h_E \geq \frac{1}{6\sigma_{\mathscr{K}}\sigma_{\mathscr{F}}} h_E^3 \ .$$

This yields together with the stability, see Definition 2.12,

$$\frac{h_{T_{\mathrm{tet}}}}{\rho_{T_{\mathrm{tet}}}} = \frac{h_{T_{\mathrm{tet}}} A_{T_{\mathrm{tet}}}}{3 V_{T_{\mathrm{tet}}}} \leq \frac{4\sigma_{\mathscr{K}}\sigma_{\mathscr{F}} h_K^3}{h_E^3} \leq 4\sigma_{\mathscr{K}}\sigma_{\mathscr{F}} c_{\mathscr{K}}^3 \ .$$

In the case $l \geq 1$, the volume $V_{T_{\mathrm{tet}}}$ gets smaller. The triangle $T \subset F \in \mathscr{F}(K)$ is obtained by successive splitting of an initial triangle T_0 of the mesh with level zero. Due to the construction, these triangles are similar and the relation $|T| = |T_0|/4^l$ holds. Taking into account this relation in the considerations above gives the general estimate

$$\frac{h_{T_{\mathrm{tet}}}}{\rho_{T_{\mathrm{tet}}}} \leq \sigma_{\mathrm{tet}} \quad \text{with} \quad \sigma_{\mathrm{tet}} = 4^{l+1}\sigma_{\mathscr{K}}\sigma_{\mathscr{F}} c_{\mathscr{K}}^3 \ .$$

□

Similar to the two-dimensional case we obtain the following two results on the object counts. In the corollary for three space dimensions, however, we additionally assume the stability of the mesh in contrast to the lower dimensional setting.

Corollary 2.15 *Let $\mathscr{K}_h$ be a regular and stable mesh. Every node belongs to a uniformly bounded number of elements, i.e. $|\{K \in \mathscr{K}_h : \mathbf{z} \in \mathscr{N}(K)\}| \leq c$, $\forall \mathbf{z} \in \mathscr{N}_h$. The constant $c > 0$ only depends on $\sigma_{\mathscr{K}}$, $\sigma_{\mathscr{F}}$ and $c_{\mathscr{K}}$.*

Proof According to the previous Lemma 2.14, the auxiliary discretization $\mathscr{T}_0(\mathscr{K}_h)$ is shape-regular in the sense of Ciarlet. Therefore, each node in the mesh $\mathscr{K}_h$ belongs to a uniformly bounded number of auxiliary tetrahedra, and consequently to a probably smaller uniformly bounded number of polyhedral elements. □

Lemma 2.16 *Let $\mathscr{K}_h$ be a regular and stable mesh. Every element contains a uniformly bounded number of nodes, edges and faces, i.e.*

$$|\mathscr{N}(K)| \leq c \ , \quad |\mathscr{E}(K)| \leq c \ , \quad |\mathscr{F}(K)| \leq c \ , \quad \forall K \in \mathscr{K}_h \ .$$

The constants $c > 0$ only depend on $\sigma_{\mathscr{K}}$, $\sigma_{\mathscr{F}}$ and $c_{\mathscr{K}}$.

Proof For the surface area of a polytopal element $K \in \mathscr{K}_h$, we have due to the regularity and stability of the mesh

$$|\partial K| = \sum_{F \in \mathscr{F}(K)} |F| \geq |\mathscr{F}(K)|\, \pi \frac{h_K^2}{c_{\mathscr{K}}^2 \sigma_{\mathscr{F}}^2} ,$$

see Remark 2.13. Using the auxiliary discretization into tetrahedra T_{tet} with corresponding triangles $T \in \mathscr{T}_0(\partial K)$, for which $|T| \leq 3V_{\text{tet}}/\rho_K$ since $V_{\text{tet}} = \frac{1}{3}\operatorname{alt}(T_{\text{tet}}, T)|T|$, we obtain on the other hand

$$|\partial K| = \sum_{T \in \mathscr{T}_0(\partial K)} |T| \leq \sum_{T \in \mathscr{T}_0(\partial K)} \frac{3V_{\text{tet}}}{\rho_K} = \frac{3|K|}{\rho_K} \leq 3\sigma_{\mathscr{K}} h_K^2 ,$$

due to $|K| \leq h_K^3$ and the regularity. Thus, the number of faces is uniformly bounded, namely $|\mathscr{F}(K)| \leq 3\sigma_{\mathscr{K}} c_{\mathscr{K}}^2 \sigma_{\mathscr{F}}^2/\pi$. According to Lemma 2.7, each of these faces has a uniformly bounded number of nodes and edges. Consequently, the number of nodes and edges of the element K is also uniformly bounded. □

If only the regularity of a polyhedral mesh is assumed, the auxiliary discretization of tetrahedra is not necessarily regular. The edges might degenerate without the stability and thus, the condition on the aspect ratio for the tetrahedra does not hold anymore. But, the stability can be weakend such that the tetrahedral mesh still satisfies a maximum angle condition.

Definition 2.17 (Weakly Stable Mesh in 3D) The family of meshes $\mathscr{K}_h$ is called weakly stable if there is a constant $c_{\mathscr{F}} > 0$ such that for all polygonal faces $F \in \mathscr{F}_h$ in the mesh and all its edges $E \in \mathscr{E}(F)$ it holds

$$h_F \leq c_{\mathscr{F}} h_E .$$

In contrast to stable meshes, the edges of elements in weakly stable meshes might degenerate with respect to the element diameter. But, due to the weak stability, small edges involve that adjacent faces are also small in their size. Thus, if an edge degenerates to a point, the adjacent faces will degenerate to this point, too. A consequence of this definition is, that the polygonal faces in a regular and weakly stable mesh are regular and stable in the two-dimensional sense.

Lemma 2.18 *Let $K \in \mathscr{K}_h$ be an element of a regular and weakly stable polyhedral mesh $\mathscr{K}_h$. The auxiliary discretization of tetrahedra $\mathscr{T}_l(K)$ and $\mathscr{T}_l(\mathscr{K}_h)$ satisfy a maximum angle condition, i.e., all dihedral angles between faces and all angles within a triangular face are uniformly bounded from above by a constant which is strictly less than π. The maximum angle only depends on $\sigma_{\mathscr{K}}$, $\sigma_{\mathscr{F}}$, $c_{\mathscr{F}}$ and the mesh level l in the face discretization.*

Proof Similar as in the proof of Lemma 2.14, we only consider $l = 0$. The general case $l > 0$ follows due to the fact that the triangles in the face triangulation $\mathscr{T}_l(F)$

are similar to those in $\mathscr{T}_0(F)$. Thus, the arguments turn over and the dependence on l enters the constants. In order to prove the maximum angle condition for the tetrahedral mesh, we distinguish several cases. First we show that the angles in the surface triangles of the tetrahedra are bounded uniformly by a constant strictly less than π. Afterwards, we bound the dihedral angles.

Let $T_{\text{tet}} \in \mathscr{T}_0(K)$ be a tetrahedra and T one of its triangular faces. If $T \in \mathscr{T}_0(F)$ for a face $F \in \mathscr{F}(K)$, then all angles of T are bounded uniformly from above by a constant strictly less than π depending only on $\sigma_{\mathscr{F}}$ according to Lemma 2.8, since F is a regular polygon. On the other hand, if $T \subset K$, we consider the intersection of the polyhedral element K with the plane in which T lies. The intersection is obviously a polygon and we denote it by P. Since K is star-shaped with respect to a ball of radius ρ_K and center $\mathbf{z}_K$, we easily see that P is star-shaped with respect to the enclosed circle of radius ρ_K and center $\mathbf{z}_K$. Thus, P is a regular polygon because of

$$\frac{h_P}{\rho_P} \leq \frac{h_K}{\rho_K} \leq \sigma_{\mathscr{K}} \ .$$

Consequently, T is part of an auxiliary triangulation of a regular polygonal element and thus its angles are bounded from above according to Lemma 2.8 by a constant depending only on $\sigma_{\mathscr{K}}$.

Next, we consider the dihedral angles of T_{tet}. Let T_i, $i = 1, 2, 3, 4$ be the triangular faces of T_{tet} and $E_{ij} = \overline{T_i} \cap \overline{T_j}$ be the edge shared by the triangles T_i and T_j for $i \neq j$. Furthermore, let the triangles be numbered such that $T_1 \in \mathscr{T}_0(F)$ for some face $F \in \mathscr{F}(K)$ and $T_i \subset K$ for $i = 2, 3, 4$. We distinguish again two cases. First, consider the dihedral angle between $T_1 \subset \partial K$ and $T_i \subset K$, $i = 2, 3, 4$. We denote the dihedral angle by δ. It is given in the plane orthogonal to E_{1i} as the angle between the two planes spanned by T_1 and T_i. Without loss of generality let $\mathbf{z}_K$ lie on the plane orthogonal to E_{1i} and denote by $\mathbf{y}$ the intersection of all three planes, see Fig. 2.5. For $\delta \geq \pi/2$, it is

$$\delta = \frac{\pi}{2} + \arccos\left(\frac{h_a}{|\mathbf{y} - \mathbf{z}_K|}\right) ,$$

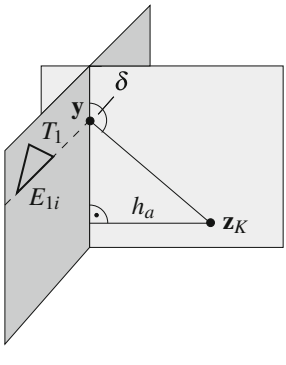

Fig. 2.5 The altitude $h_a = \text{alt}(T_{\text{tet}}, T_1)$, intersection point $\mathbf{y}$ and demonstration of dihedral angle δ in plane orthogonal to the edge E_{ij} through $\mathbf{z}_K$ between the triangles T_1 and T_i as described in the proof of Lemma 2.18

where $h_a = \operatorname{alt}(T_{\text{tet}}, T_1)$ is the altitude of the tetrahedron T_{tet} with respect to the side T_1, which corresponds to the distance of $\mathbf{z}_K$ to the plane through T_1. Consequently, it is $h_a \geq \rho_K$ due to the regularity of the polyhedral element K. Furthermore, K is enclosed by a sphere of radius h_K and center $\mathbf{z}_K$. Since $\mathbf{y}$ is the orthogonal projection of $\mathbf{z}_K$ onto the line through E_{1i}, its distance to $\mathbf{z}_K$ is smaller than the distance of z_K to the edge, thus $|\mathbf{y} - \mathbf{z}_K| \leq h_K$. This yields

$$\frac{h_a}{|\mathbf{y} - \mathbf{z}_K|} \geq \frac{\rho_K}{h_K} \geq \frac{1}{\sigma_{\mathscr{K}}} ,$$

because of the regularity. Since arc cosine is monotonically decreasing, we obtain

$$\delta \leq \frac{\pi}{2} + \arccos\left(\frac{1}{\sigma_{\mathscr{K}}}\right) < \pi .$$

It remains to bound the dihedral angle between triangular faces of the tetrahedra with $T_i, T_j \subset K$. We denote the angle again by δ. According to Proposition 3.1 in [122], the volume $V_{T_{\text{tet}}}$ of T_{tet} satisfy the relation

$$V_{T_{\text{tet}}} = \frac{2}{3h_{E_{ij}}} |T_i| \, |T_j| \, \sin\delta .$$

On the other hand it is

$$V_{T_{\text{tet}}} = \frac{1}{3} \operatorname{alt}(T_{\text{tet}}, T_1) \, |T_1| .$$

If we assume $\pi/2 \leq \delta \leq \pi$, this yields

$$\delta = \frac{\pi}{2} + \arccos\left(\frac{h_{E_{ij}} \operatorname{alt}(T_{\text{tet}}, T_1) \, |T_1|}{2|T_i| \, |T_j|}\right) . \tag{2.5}$$

The areas of the triangles are given by

$$|T_\ell| = \frac{1}{2} h_{E_{ij}} \operatorname{alt}(T_\ell, E_{ij}) \quad \text{for } \ell = i, j .$$

Obviously, the altitude $\operatorname{alt}(T_\ell, E_{ij})$ is smaller than the edge shared by T_ℓ and T_1 and thus smaller than the diameter of T_1. This yields

$$|T_\ell| \leq \frac{1}{2} h_{E_{ij}} h_{E_{1\ell}} \leq \frac{1}{2} h_{E_{ij}} h_{T_1} \quad \text{for } \ell = i, j .$$

Furthermore, it is $\operatorname{alt}(T_{\text{tet}}, T_1) \geq \rho_K$ and $h_{E_{ij}} \leq h_K$. Consequently, we obtain for the argument in the arc cosine in (2.5)

$$\frac{h_{E_{ij}} \operatorname{alt}(T_{\text{tet}}, T_1) |T_1|}{2|T_i||T_j|} \geq \frac{2 \operatorname{alt}(T_{\text{tet}}, T_1) |T_1|}{h_{E_{ij}} h_{T_1}^2} \geq \frac{2 \rho_K |T_1|}{h_K h_{T_1}^2} \geq \frac{2\pi \rho_{T_1}^2}{\sigma_{\mathscr{K}} h_{T_1}^2} ,$$

where we used the regularity of the mesh and the incircle of T_1 with radius ρ_{T_1}, which gives $|T_1| \geq \pi \rho_{T_1}^2$, in the last step. Finally, we employ the weak stability of the mesh, which ensures that the polygonal faces are regular and stable in the two-dimensional sense. Therefore, the auxiliary triangulation of the polygonal faces is regular in the sense of Ciarlet and it is $h_{T_1} / \rho_{T_1} \leq \sigma_{\mathscr{T}}$, where $\sigma_{\mathscr{T}}$ only depends on $\sigma_{\mathscr{F}}$ and $c_{\mathscr{F}}$, see Lemma 2.3. Since the arc cosine is monotonically decreasing, Eq. (2.5) yields with the previous considerations

$$\delta \leq \frac{\pi}{2} + \arccos\left(\frac{2\pi \rho_{T_1}^2}{\sigma_{\mathscr{K}} h_{T_1}^2}\right) \leq \frac{\pi}{2} + \arccos\left(\frac{2\pi}{\sigma_{\mathscr{K}} \sigma_{\mathscr{T}}^2}\right) < \pi .$$

In summary, all angles in the surface triangles of the tetrahedra and all dihedral angles between faces are bounded by constants that are strictly less than π. Taking the maximum of them proves the maximal angle condition for the auxiliary discretization of tetrahedra. □

2.2.3 *Mesh Refinement*

Although the use of polygonal and polyhedral meshes is quite interesting for practical applications, only a few commercial mesh generators are able to create and refine such general meshes. For the two-dimensional case there is the free MATLAB tool PolyMesher available, see [167], and in three-dimensions one often exploits either Voronoi meshes, see [70], or dual meshes to given tetrahedral discretizations. In the following, we assume that a polygonal or polyhedral mesh is given and we address the refinement of such meshes. We may perform uniform refinement, where all elements of a mesh are refined, or adaptive refinement, where only a few elements are refined according to some criterion. For polygonal and polyhedral meshes, there is a great flexibility for the refinement process. We do not have to take care on hanging nodes and edges, since they are naturally included in such meshes.

For the refinement process, we choose the bisection of elements. For the description of the procedure, we focus on a single polygonal or polyhedral element $K \subset \mathbb{R}^d$, $d = 2, 3$. Furthermore, we assume that K is convex. The method might be adapted to non-convex, star-shaped elements, but this would yield several special cases which shall be omitted here. In order to obtain some geometrical information

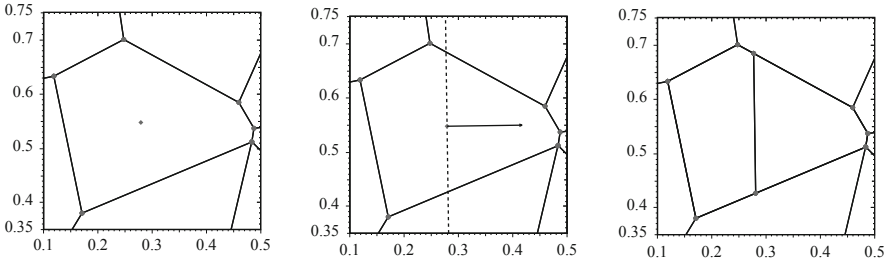

Fig. 2.6 Refinement of an element: element with center $\bar{\mathbf{x}}_K$ (left), element with eigenvector (middle), two new elements (right)

of the element shape, we first compute the covariance matrix

$$M_{\mathrm{Cov}}(K) = \frac{1}{|K|} \int_K (\mathbf{x} - \bar{\mathbf{x}}_K)(\mathbf{x} - \bar{\mathbf{x}}_K)^\top \mathrm{d}\mathbf{x} \,,$$

where

$$\bar{\mathbf{x}}_K = \frac{1}{|K|} \int_K \mathbf{x} \, \mathrm{d}\mathbf{x}$$

is the barycenter of the element. The matrix $M_{\mathrm{Cov}}(K) \in \mathbb{R}^{d \times d}$ is symmetric and positive definite due to construction. We compute its eigenvalues and the corresponding eigenvectors. This principle component analysis provides some information on the dimensions of the element. The square root of the eigenvalues give the standard deviation in the direction of the corresponding eigenvector. Thus, the eigenvector which belongs to the biggest eigenvalue points into the direction of the longest extend of the element K. Consequently, we split the element orthogonal to this eigenvector through the barycenter $\bar{\mathbf{x}}_K$ of K, see Fig. 2.6. Afterwards, two new elements are obtained. This strategy actually works in any dimension $d \in \mathbb{N}$. Similar ideas are used in [144] to cluster point clouds which are used for matrix approximation in fast boundary element methods.

Figure 2.7 shows the uniform refinement starting from a triangle. The meshes are obtained after one, three, five and seven refinement steps. We recognize that even a refinement of a triangle results in an unstructured polygonal mesh. Nevertheless, the resulting sequence of meshes has a uniform character. A big advantage of the introduced strategy can be seen in an adaptive context. It is possible to perform local refinements within a few elements. Classical mesh refinement techniques for triangular meshes, for example, suffer from the fact that local refinement propagates into neighbouring regions. This behaviour is necessary since the resulting meshes have to be admissible and thus the use of hanging nodes is very restricted or even avoided.

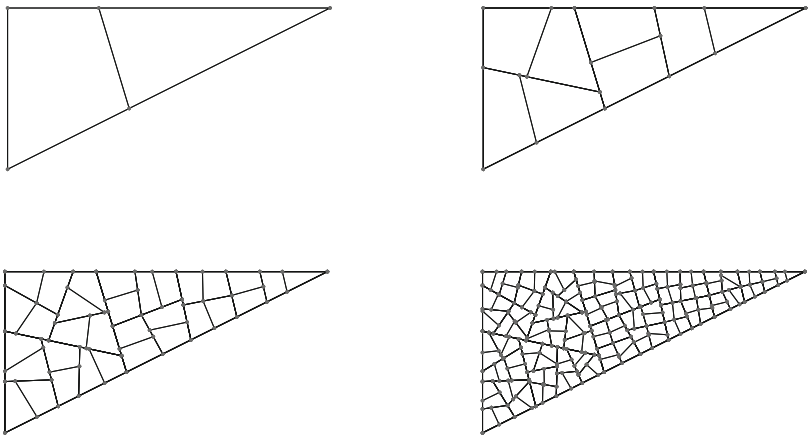

Fig. 2.7 Uniform refinement of a triangle after one, three, five and seven refinement steps

Finally, the question arises whether the regularity and the stability of a mesh is preserved during the refinement. In general this is not possible with the prescribed procedure. During the bisection of elements, small edges and thin faces might occur. However, the aspect ratios for convex elements stay bounded, since the algorithm tries to equilibrate the extend of the element in its characteristic directions. Thus, the regularity is preserved for convex elements in two-dimensions. The stability, however, has to be enforced during the refinement process if it is needed. The introduced bisection strategy for mesh refinement is applied in most of the numerical experiments presented in this book.

2.3 Trefftz-Like Basis Functions

Our goal is to introduce finite dimensional spaces V_h^k over polygonal and polyhedral discretizations of the domain $\Omega \subset \mathbb{R}^d$, $d = 2, 3$, which approximate the Sobolev space $H^1(\Omega)$. The index $k \in \mathbb{N}$ denotes the order of the approximation space. In this section, a more general strategy is presented which extends the original idea in [146] to arbitrary order. The approximation space $V_h^k = \text{span } \Psi_h^k$ is constructed as span of some basis Ψ_h^k. For $d = 2$, this basis is specified in the following and consists of nodal, edge and element basis functions. These functions are indicated by $\psi_{\mathbf{z}}$, ψ_E and ψ_K, respectively. All of them have certain degrees and thus they are marked and numbered by indices like $\psi_{E,i}$ and $\psi_{K,i,j}$ for some i, j. However, for shorter notation, we will skip sometimes parts of the indices if the meaning is

clear from the context and we just write ψ, ψ_i and $\psi_{i,j}$, for example. For the three-dimensional case with $d = 3$, the ideas will be generalized and we have additional face basis functions.

The basis functions are defined element-wise by local solutions of boundary value problems in the spirit of Trefftz [168]. The diffusion equation in mind, we utilize Laplace and Poisson equations over each element with Dirichlet boundary data to construct the basis functions. Due to the local Dirichlet boundary conditions, the traces of the basis functions will be continuous across element interfaces, i.e. they are H^1-conforming. In the following, we first introduce the two-dimensional case in the Sects. 2.3.1–2.3.3. Afterwards, a simple generalization to three-dimensions is given in Sect. 2.3.4, which builds on the previous considerations.

2.3.1 Node and Edge Basis Functions

Let $\mathscr{K}_h$ be a polygonal mesh of a bounded domain $\Omega \subset \mathbb{R}^2$. The functions $\psi_{\mathbf{z}}$ and ψ_E, which are assigned to nodes and edges, are defined to satisfy the Laplace equation on each element. Their Dirichlet trace on the element boundaries is chosen to be continuous and piecewise polynomial. Thus, we define for each node $\mathbf{z} \in \mathscr{N}_h$ the basis function $\psi_{\mathbf{z}}$ as unique solution of

$$\begin{aligned} -\Delta \psi_{\mathbf{z}} &= 0 \quad \text{in } K \quad \text{for all } K \in \mathscr{K}_h \,, \\ \psi_{\mathbf{z}}(\mathbf{x}) &= \begin{cases} 1 & \text{for } \mathbf{x} = \mathbf{z} \,, \\ 0 & \text{for } \mathbf{x} \in \mathscr{N}_h \setminus \{\mathbf{z}\} \,, \end{cases} \\ \psi_{\mathbf{z}} &\text{ is linear on each edge of the mesh} \,. \end{aligned} \tag{2.6}$$

So, the function $\psi_{\mathbf{z}}$ is locally defined as solution of a boundary value problem over each element. If the element $K \in \mathscr{K}_h$ is convex, the boundary value problem can be understood in the classical sense and it is $\psi_{\mathbf{z}} \in C^2(K) \cap C^0(\overline{K})$, see [82, 87]. However, we explicitly allow star-shaped elements within the discretization $\mathscr{K}_h$ of the domain Ω. In this case, the boundary value problem is understood in the weak sense and we obtain $\psi_{\mathbf{z}} \in H^1(K)$. Since the Dirichlet trace is continuous across element interfaces, the local regularity of $\psi_{\mathbf{z}}$ yields $\psi_{\mathbf{z}} \in H^1(\Omega)$. This will also be true for the edge and element basis functions. In the following, the local problems for the definition of basis functions are always understood in the classical or weak sense depending on the shape of the elements. In contrast to [146], we only make use of the fact that the nodal, edge and element basis functions satisfy $\psi \in H^1(K)$ for $K \in \mathscr{K}_h$ and we do not use a maximum principle [82, 140] for harmonic functions which would require convex elements.

In the case that $\mathscr{K}_h$ is an admissible triangulation without hanging nodes, the basis functions turn out to be the standard hat functions of classical finite element methods. This relation is quite obvious since the lowest order linear basis functions satisfy the data on the boundary of each element and they are harmonic because of their linearity. According to the unique solvability of the Dirichlet problem for the Laplace equation the hat functions coincide with the basis functions defined here. In this sense, the BEM-based FEM can be seen as a generalization of standard finite element methods.

If $\mathscr{K}_h$ is a polygonal mesh containing only convex elements, another connection can be recognized. For the model problem, we rediscover the so called harmonic coordinates mentioned in several articles like [77, 84, 112, 126]. These harmonic coordinates restricted to one element $K \in \mathscr{K}_h$ are a special type of barycentric coordinates, i.e., they satisfy

$$\psi_{\mathbf{z}}(\mathbf{x}) \geq 0 \quad \text{on } \overline{K} \tag{2.7}$$

for $\mathbf{z} \in \mathscr{N}(K)$ and it is

$$v = \sum_{\mathbf{z} \in \mathscr{N}(K)} v(\mathbf{z}) \psi_{\mathbf{z}} \tag{2.8}$$

for any linear function v on $\overline{K}$ according to [84]. Condition (2.7) follows directly from the minimum-maximum principle [82, 140]. To verify (2.8), we observe that both sides of the equation are harmonic and coincide on the boundary of K. Therefore, the difference of both sides is harmonic and identical to zero on the boundary. Using the minimum-maximal principle again shows that Eq. (2.8) is valid in the whole element. In [76, 77], the authors have proven for any set of barycentric coordinates and especially for the harmonic coordinates, which are considered in this section, that they satisfy the estimate

$$0 \leq L_{\mathbf{z}}^{\text{low}} \leq \psi_{\mathbf{z}} \leq L_{\mathbf{z}}^{\text{up}} \leq 1 \quad \text{on } \overline{K}$$

for $\mathbf{z} \in \mathscr{N}(K)$. Here, $L_{\mathbf{z}}^{\text{low}}$ and $L_{\mathbf{z}}^{\text{up}}$ are piecewise linear functions defined as follows. Both functions are equal to one at the node $\mathbf{z}$ and they are equal to zero at every other node on the boundary of K. Additionally, $L_{\mathbf{z}}^{\text{low}}$ is linear on the triangle constructed by connecting the node before and after $\mathbf{z}$ on the boundary, and zero else, see Fig. 2.8. The function $L_{\mathbf{z}}^{\text{up}}$ is linear on each triangle that is obtained by connecting $\mathbf{z}$ with all other nodes on the boundary of K.

To introduce the edge basis functions ψ_E, polynomial data is prescribed on the element boundaries. Therefore, we first review a hierarchical polynomial basis over the interval $[0, 1]$. We set

$$p_0(t) = t \qquad \text{and} \qquad p_1(t) = 1 - t \qquad \text{for } t \in [0, 1] \,,$$

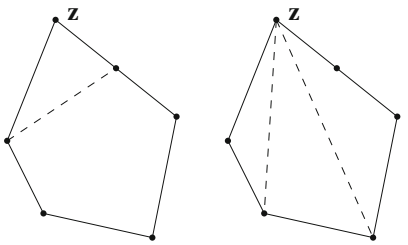

Fig. 2.8 Triangles for construction of $L_{\mathbf{z}}^{\text{low}}$ (left) and $L_{\mathbf{z}}^{\text{up}}$ (right)

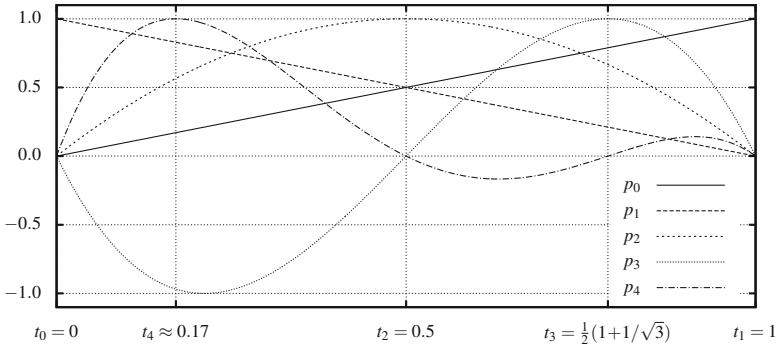

Fig. 2.9 Visualization of p_i for $i = 0, \ldots, 4$

and assign these functions to the points $t_0 = 0$ and $t_1 = 1$, respectively. Afterwards, we define $p_i \in \mathscr{P}^i([0,1])$, $i \geq 2$ with exact degree i recursively as

$$p_i = \frac{\widetilde{p}_i}{\widetilde{p}_i(t_i)} ,$$

where $\widetilde{p}_i \in \mathscr{P}^i([0,1]) \setminus \{0\}$ is a polynomial with $\widetilde{p}_i(t_j) = 0$ for $j = 0, \ldots, i-1$ and

$$t_i = \max\{\arg\max_{t \in [0,1]} |\widetilde{p}_i(t)|\} .$$

The polynomial p_i is well defined since $\widetilde{p}_i$ is unique up to a multiplicative constant and we obviously have $t_i \neq t_j$ for $j < i$. In Fig. 2.9, the first polynomials are visualized. One easily sees that these polynomials are linearly independent and that for $k \geq 1$

$$\mathscr{P}^k([0,1]) = \operatorname{span}\{p_i : i = 0, \ldots, k\} .$$

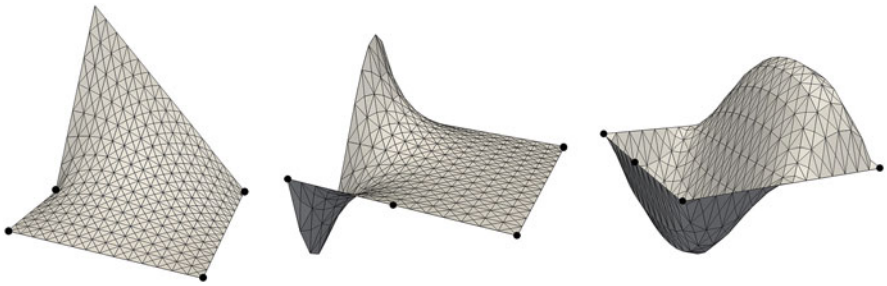

Fig. 2.10 Visualization of $\psi_{\mathbf{z}}$, $\psi_{E,3}$ and $\psi_{K,1,0}$ over rectangular element with additional node on straight line, nodes are marked with black dots

For the definition of edge basis functions ψ_E, we make use of a linear parametrization of the corresponding edge. Let $E \in \mathscr{E}_h$ with $E = \overline{\mathbf{z}_b \mathbf{z}_e}$ and

$$E : [0,1] \ni t \mapsto \mathfrak{F}_E(t) = \mathbf{z}_b + t(\mathbf{z}_e - \mathbf{z}_b) \ .$$

In contrast to nodal basis functions, we have more than one basis function per edge. We define $\psi_{E,i}$ for $i = 2, \ldots, k$ as unique solution of

$$-\Delta \psi_{E,i} = 0 \quad \text{in } K \quad \text{for all } K \in \mathscr{K}_h \ ,$$

$$\psi_{E,i} = \begin{cases} p_i \circ \mathfrak{F}_E^{-1} & \text{on } E \ , \\ 0 & \text{on } \mathscr{E}_h \setminus \{E\} \ , \end{cases}$$

and we assign these functions to the points $\mathbf{z}_{E,i} = \mathfrak{F}_E(t_i)$. In Fig. 2.10, an approximation of such a function is visualized over one rectangular element. As in the case of nodal basis functions, we observe that the Dirichlet trace is continuous along element boundaries. Thus, we have $\psi_{E,i} \in H^1(K)$ for $K \in \mathscr{K}_h$ which yields $\psi_{E,i} \in H^1(\Omega)$. With the conventions

$$\psi_{E,0} = \psi_{\mathbf{z}_b} \qquad \text{and} \qquad \psi_{E,1} = \psi_{\mathbf{z}_e} \ ,$$

we find that

$$\mathscr{P}^k(E) = \operatorname{span}\{\psi_{E,i}\big|_E : i = 0, \ldots, k\}$$

and

$$\psi_{E,i}(\mathbf{z}_{E,j}) = \delta_{ij} \quad \text{for } j = 0, \ldots, i \ ,$$

where δ_{ij} is the Kronecker symbol. According to the last property, the functions $\psi_{\mathbf{z}}$ and $\psi_{E,i}$ are linearly independent. So, we collect them in the basis

$$\Psi_{h,H}^k = \{\psi_{\mathbf{z}}, \psi_{E,i} : \mathbf{z} \in \mathscr{N}_h, E \in \mathscr{E}_h, i = 2, \ldots, k\} \ ,$$

and we have

$$V_{h,H}^k = \text{span } \Psi_{h,H}^k \subset H_\Delta^1(\mathscr{K}_h) \subset H^1(\Omega) \ .$$

Here, for $k = 1$, only nodal basis functions are used in $\Psi_{h,H}^k$ and for $k \in \mathbb{N}$,

$$H_\Delta^k(\mathscr{K}_h) = \left\{ v \in H^k(\Omega) : \ (\nabla v, \nabla w)_{L_2(K)} = 0 \ \forall w \in H_0^1(K), \ \forall K \in \mathscr{K}_h \right\} \tag{2.9}$$

is the space of piecewise weakly harmonic functions.

2.3.2 Element Basis Functions

Next, we address the definition of element basis functions over the polygonal mesh $\mathscr{K}_h$ of a domain $\Omega \subset \mathbb{R}^2$. To motivate the procedure, we remember that the nodal and edge basis functions satisfy the Laplace equation inside the elements and are polynomial on the edges. The nodal functions $\psi_{\mathbf{z}}$ are linear on edges, and thus they satisfy the one dimensional Laplace equation along edges: $\Delta_1 \psi_{\mathbf{z}} = 0$ on $E \in \mathscr{E}_h$. If we compute the 1D-Laplacian of the edge functions ψ_E along the edge E, we observe that $\Delta_1 \psi_{E,i} \in \mathscr{P}^{i-2}(E)$, $i \geq 2$, and thus the edge basis functions satisfy the Poisson equation with polynomial right hand side on each edge. Additionally, it is easy to check that

$$\mathscr{P}^{k-2}(E) = \text{span}\,\{\Delta_1 \psi_{E,i} : i = 2, \ldots, k\}$$

for $k \geq 2$. From this point of view, we exchanged the Laplace equation for the Poisson equation on the edges as we have made the step from nodal to edge basis functions. The same is done for the element basis functions. Here, we exchange the Laplace for the Poisson equation in the elements and we prescribe right hand sides such that they form a basis of $\mathscr{P}^{k-2}(K)$. Thus, we define $\psi_{K,i,j}$ for $K \in \mathscr{K}_h$, $i = 0, \ldots, k-2$ and $j = 0, \ldots, i$ as unique solution of

$$\begin{aligned} -\Delta \psi_{K,i,j} &= p_{K,i,j} \quad \text{in } K \ , \\ \psi_{K,i,j} &= 0 \qquad\quad \text{else} \ , \end{aligned} \tag{2.10}$$

where

$$\mathscr{P}^{k-2}(K) = \text{span}\,\{p_{K,i,j} : i = 0, \ldots, k-2 \text{ and } j = 0, \ldots, i\} \ . \tag{2.11}$$

Consequently, we have $\frac{1}{2}k(k-1)$ element basis functions per element. The support of such a function is limited to one element, i.e. supp $\psi_{K,i,j} = \overline{K}$, and the function

itself belongs to $H_0^1(K)$. Due to the local regularity, we obtain $\psi_{K,i,j} \in H^1(\Omega)$. See Fig. 2.10 for a visualization of such an element basis function.

Remark 2.19 In the numerical experiments we will choose the polynomial basis as shifted monomials, namely as

$$p_{K,i,j}(\mathbf{x}) = \left(x_1 - z_{K,1}\right)^{i-j} \left(x_2 - z_{K,2}\right)^{j}, \quad \mathbf{x} = \left(x_1, x_2\right)^{\top} \in K ,$$

where $\mathbf{z}_K = \left(z_{K,1}, z_{K,2}\right)^{\top}$ is given in Definition 2.1. For $i, j = 0$, the element bubble function from [146] is recovered, since $p_{K,0,0} = 1$.

We define the set of functions

$$\Psi_{h,B}^k = \{\psi_{K,i,j} : K \in \mathscr{K}_h, i = 0, \ldots, k-2 \text{ and } j = 0, \ldots, i\}$$

and the space

$$V_{h,B}^k = \text{span } \Psi_{h,B}^k \subset H^1(\Omega) ,$$

which consists of element bubble functions that vanish on the skeleton of the mesh. For $k = 1$, this means $\Psi_{h,B}^k = \varnothing$. Furthermore, we point out that the definition of element basis functions $\psi_{K,i,j} \in \Psi_{h,B}^k$ is equivalent to the variational formulation

$$\begin{aligned} &\text{Find } \psi_{K,i,j} \in H_0^1(K) : \\ &\left(\nabla\psi_{K,i,j}, \nabla w\right)_{L_2(K)} = \left(p_{K,i,j}, w\right)_{L_2(K)} \quad \forall w \in H_0^1(K). \end{aligned} \tag{2.12}$$

Lemma 2.20 *The functions in $\Psi_{h,B}^k$ are linearly independent.*

Proof Since the support of an element basis function is restricted to one element, the functions belonging to different elements are independent. Therefore, it is sufficient to consider just functions over one element in this proof. Let $\alpha_{i,j} \in \mathbb{R}$ for $i = 0, \ldots, k-2$ and $j = 0, \ldots, i$ and let $\sum_{i,j} \alpha_{i,j}\psi_{i,j} = 0$. Consequently, we have $\sum_{i,j} \alpha_{i,j}\nabla\psi_{i,j} = 0$. Due to this and since the element basis functions $\psi_{i,j} = \psi_{K,i,j}$ satisfy (2.12), we obtain

$$\Big(\sum_{i,j} \alpha_{i,j} p_{i,j}, w\Big)_{L_2(K)} = \Big(\sum_{i,j} \alpha_{i,j} \nabla\psi_{i,j}, \nabla w\Big)_{L_2(K)} = 0 \quad \text{for } w \in H_0^1(K) .$$

The function space $C_0^\infty(K)$ is dense in $H_0^1(K)$ and thus the fundamental lemma of the calculus of variations yields $\sum_{i,j} \alpha_{i,j} p_{i,j} = 0$. Because of the choice of $p_{i,j}$ as basis of $\mathscr{P}^{k-2}(K)$, it follows that $\alpha_{i,j} = 0$ for $i = 0, \ldots, k-2$ and $j = 0, \ldots, i$. □

2.3.3 Final Approximation Space

The final basis for the approximation space of $H^1(\Omega)$ is now defined as

$$\Psi_h^k = \Psi_{h,H}^k \cup \Psi_{h,B}^k \ ,$$

and combines the nodal, edge and element basis functions. All functions in $\Psi_{h,H}^k$ locally satisfy the Laplace equation on each element and so, they are piecewise harmonic in a weak sense. Different from the functions in $\Psi_{h,H}^k$, the functions in $\Psi_{h,B}^k$ are exactly those which are not locally harmonic. They obviously serve the approximation of non-harmonic functions. Furthermore, we observe that

$$(\nabla\psi, \nabla\varphi)_{L_2(K)} = 0 \quad \text{for } \psi \in \Psi_{h,H}^k,\ \varphi \in \Psi_{h,B}^k \ , \tag{2.13}$$

since $\psi \in H^1_\Delta(\mathscr{K}_h)$ and $\varphi \in H^1_0(K)$, cf. (2.9). Sometimes, we will consider the basis functions restricted to a single element. For this reason, we define for $K \in \mathscr{K}_h$

$$\Psi_h^k\big|_K = \left\{ \psi\big|_K : \psi \in \Psi_h^k \right\}$$

and $\Psi_{h,H}^k\big|_K$ as well as $\Psi_{h,B}^k\big|_K$ accordingly. The final approximation space is conforming, i.e.

$$V_h^k = \operatorname{span} \Psi_h^k \subset H^1(\Omega) \ ,$$

and can be written as a direct sum of piecewise weakly harmonic functions and element bubble functions. The space of element bubble functions can be further decomposed into its contributions from the single elements, because of the zero traces on the element boundaries. Thus, it is

$$V_h^k = V_{h,H}^k \oplus V_{h,B}^k \quad \text{with} \quad V_{h,B}^k = \bigoplus_{K \in \mathscr{K}_h} V_{h,B}^k\big|_K \ ,$$

where the same notation holds for the restriction to a single element as above. A simple counting argument shows that

$$\dim V_h^k\big|_K = k\,|\mathscr{N}(K)| + \tfrac{1}{2}k(k-1) \ ,$$

since

$$\dim V_{h,H}^k\big|_K = k\,|\mathscr{N}(K)| \quad \text{and} \quad \dim V_{h,B}^k\big|_K = \binom{d+k-2}{d} = \tfrac{1}{2}k(k-1) \ .$$

Due to the construction of the basis, it is easily seen that the approximation space can be written in the following form

$$V_h^k = \left\{ v \in H^1(\Omega) : \Delta v \in \mathscr{P}^{k-2}(K) \text{ and } v|_{\partial K} \in \mathscr{P}^k_{\mathrm{pw}}(\partial K) \ \forall K \in \mathscr{K}_h \right\}$$

with the convention $\mathscr{P}^{-1}(K) = \{0\}$. Thus, the functions in V_h^k are polynomials of degree k over each edge and their Laplacian over each element is a polynomial of degree $k-2$.

The virtual element method (VEM) in [25] also uses this approximation space. Therefore, the BEM-based FEM and the VEM seek the approximation of the solution of the boundary-value problem for the diffusion Eq. (2.1) in the same discrete space. The VEM reduces all computations to carefully chosen degrees of freedom and to local projections into polynomial spaces. The BEM-based FEM in contrary makes use of the explicit knowledge of the basis functions and thus enables the evaluation of the approximation inside the elements. Both methods rely on clever reformulations to avoid volume integration. Since the BEM-based FEM applies Trefftz-like basis functions, which are related to the differential equation of the global problem, the discrete space for the BEM-based FEM and the VEM differ as soon as more general boundary-value problems are considered.

2.3.4 Simple Generalization to 3D

This section gives a straight forward generalization to the three-dimensional case. A more involved one is postponed to a later chapter. Let $\mathscr{K}_h$ be a polyhedral mesh of a bounded domain $\Omega \subset \mathbb{R}^3$. We restrict ourselves here to polyhedral elements that have triangular faces. This can be always achieved by triangulating the polygonal faces of general polyhedra. For this purpose we may use the auxiliary triangulation $\mathscr{T}_0(\partial K)$ introduced in Sect. 2.2.2 and reinterpret K as element with triangular faces. Consequently, one additional node per face is introduced on the surface of the polyhedral element K. Several constructed triangular faces meet in this node and lie on a flat part of ∂K. However, the notion of polyhedral elements allows for such degenerations. A more direct approach for the treatment of polygonal faces will be discussed in Sect. 6.2.

Turning to the construction of the approximation space V_h^k in three-dimensions, we may recognize that it can be written down immediately as

$$V_h^k = \left\{ v \in H^1(\Omega) : \Delta v \in \mathscr{P}^{k-2}(K) \text{ and } v|_{\partial K} \in \mathscr{P}^k_{\mathrm{pw}}(\partial K) \ \forall K \in \mathscr{K}_h \right\} .$$

Thus, the only difference to the two-dimensional case is that the functions in V_h^k are now piecewise polynomial of degree k over the triangular faces of polyhedra instead of piecewise polynomials over the edges of polygonal elements. Consequently, the

considerations from the previous sections can be directly generalized to polyhedral meshes $\mathscr{K}_h$, for which the set of faces $\mathscr{F}_h$ consists of triangles only.

The space V_h^k is again constructed as a direct sum of piecewise weakly harmonic functions with polynomial traces on the faces of the mesh and element bubble functions that vanish on the skeleton but have a polynomial Laplacian inside the elements, i.e.

$$V_h^k = V_{h,H}^k \oplus V_{h,B}^k \quad \text{and} \quad V_{h,B}^k = \bigoplus_{K \in \mathscr{K}_h} V_{h,B}^k\big|_K \, .$$

Let $v_h = v_{h,H} + v_{h,B} \in V_h^k$ with $v_{h,H} \in V_{h,H}^k$ and $v_{h,B} \in V_{h,B}^k$. For each element $K \in \mathscr{K}_h$, it holds

$$-\Delta v_{h,H} = 0 \quad \text{in } K \quad \text{and} \quad v_{h,H} = p_{\partial K} \quad \text{on } \partial K \, , \tag{2.14}$$

as well as

$$-\Delta v_{h,B} = p_K \quad \text{in } K \quad \text{and} \quad v_{h,B} = 0 \quad \text{on } \partial K \, , \tag{2.15}$$

for some $p_{\partial K} \in \mathscr{P}^k_{\mathrm{pw}}(\partial K)$ and $p_K \in \mathscr{P}^{k-2}(K)$. Thus, $v_{h,H}$ and $v_{h,B}$ are uniquely defined by the polynomial data $p_{\partial K}$ and p_K, respectively. Consequently, the basis Ψ_h^k of V_h^k is constructed in an element-wise fashion respecting the direct sum, such that

$$\Psi_h^k\big|_K = \Psi_{h,H}^k\big|_K \cup \Psi_{h,B}^k\big|_K \quad \text{for} \quad V_h^k\big|_K = V_{h,H}^k\big|_K \oplus V_{h,B}^k\big|_K \, .$$

We choose a basis for $\mathscr{P}^k_{\mathrm{pw}}(\partial K)$ and $\mathscr{P}^{k-2}(K)$. For each function in these sets a harmonic basis function and an element basis function are obtained by (2.14) and (2.15), respectively. Due to this construction, a simple counting argument shows that

$$\dim V_h^k\big|_K = |\mathscr{N}(K)| + (k-1)|\mathscr{E}(K)| + \tfrac{1}{2}(k-1)(k-2)|\mathscr{F}(K)| + \tfrac{1}{6}k(k-1)(k+1) \, ,$$

since

$$\dim V_{h,H}^k\big|_K = |\mathscr{N}(K)| + (k-1)|\mathscr{E}(K)| + \tfrac{1}{2}(k-1)(k-2)|\mathscr{F}(K)|$$

and

$$\dim V_{h,B}^k\big|_K = \binom{d+k-2}{d} = \tfrac{1}{6}k(k-1)(k+1) \, .$$

In the previous sections on the two-dimensional case, this construction has been carried out in more detail and we have given a precise choice of basis functions. For the three-dimensional case we are content with the abstract setting and pass a

detailed presentation. We point out, however, the important orthogonality property given in (2.13), which still holds on $K \in \mathscr{K}_h$, namely

$$(\nabla v_{h,H}, \nabla v_{h,B})_{L_2(K)} = 0 \quad \text{for } v_{h,H} \in V^k_{h,H},\ v_{h,B} \in V^k_{h,B}\ .$$

This is a consequence of the weakly harmonic functions, cf. (2.9), and the element bubble functions that satisfy

$$V^k_{h,H} \subset H^1_\Delta(\mathscr{K}_h) \quad \text{and} \quad V^k_{h,B} \subset \bigoplus_{K\in\mathscr{K}_h} H^1_0(K)\ .$$

Remark 2.21 For the implementation and the numerical experiments it is important to specify the choice of basis functions. As discussed above, the sets $\Psi^k_{h,H}$ and $\Psi^k_{h,B}$ are constructed by choosing a basis for $\mathscr{P}^k_{\mathrm{pw}}(\partial K)$ and $\mathscr{P}^{k-2}(K)$, respectively. It is convenient to choose the classic Lagrange elements over triangles, cf. [40, 151], for the basis of $\mathscr{P}^k_{\mathrm{pw}}(\partial K)$, whereas the basis of $\mathscr{P}^{k-2}(K)$ might be chosen according to the two-dimensional case as shifted monomials, for instance.

2.4 Interpolation Operators

In this section, we are concerned with the interpolation of function in $H^2(\Omega)$ by functions in $V^k_h = V^k_{h,H} \oplus V^k_{h,B}$. Due to the Sobolev embedding theorem it holds that $H^2(\Omega) \subset C^0(\overline{\Omega})$, see [1], and the pointwise evaluation of such functions is well defined. Thus, we may exploit nodal interpolation to some extend. The interpolation of non-smooth functions in $H^1(\Omega)$ is postponed to later considerations, see Chap. 3.

Since V^k_h is given as a direct sum of weakly harmonic and element bubble functions, it is natural to decompose the interpolation into two corresponding operators. Therefore, we study

$$\mathfrak{I}^k_h = \mathfrak{I}^k_{h,H} + \mathfrak{I}^k_{h,B} : H^2(\Omega) \to V^k_h \subset H^1(\Omega)$$

with

$$\mathfrak{I}^k_{h,H} : H^2(\Omega) \to V^k_{h,H} \subset H^1_\Delta(\mathscr{K}_h) \quad \text{and} \quad \mathfrak{I}^k_{h,B} : H^2(\Omega) \to V^k_{h,B} \subset \bigoplus_{K\in\mathscr{K}_h} H^1_0(K)\ .$$

The interpolation operators $\mathfrak{I}^k_{h,H}$ and $\mathfrak{I}^k_{h,B}$ are discussed in the following. Furthermore, it is sufficient to introduce them over a single element, since the local nature of the operators directly extend to their global definition. Thus, we restrict ourselves to a single element of a regular polytopal mesh and denote the restrictions of the operators with the same symbols.

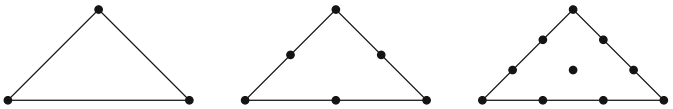

Fig. 2.11 Points for Lagrange interpolation into $\mathscr{P}^k(\partial K)$ on triangles for $k = 1, 2, 3$

We start by the interpolation into the space of weakly harmonic functions. For $v_h \in V_{h,H}^k$, it is $\Delta v_h = 0$ in K and $v|_{\partial K} \in \mathscr{P}_{\mathrm{pw}}^k(\partial K)$. Thus, for the definition of

$$\mathfrak{I}_{h,H}^k : H^2(K) \to V_{h,H}^k\big|_K \subset H_\Delta^1(K) \,,$$

we prescribe $\mathfrak{I}_{h,H}^k v|_{\partial K}$ to be equal to a standard nodal interpolation operator into the space $\mathscr{P}_{\mathrm{pw}}^k(\partial K)$ on the boundary of the polytopal element K. Afterwards, we extend this boundary data harmonically into K. By fixing a standard interpolation operator on ∂K, the operator $\mathfrak{I}_{h,H}^k$ is uniquely defined. For this purpose, we exploit the classical Lagrange interpolation on equidistant points along the edges in the boundary of polygonal elements ($d = 2$) and on equidistributed points, see Fig. 2.11, in the triangular faces in the boundary of polyhedral elements ($d = 3$). Consequently, $\mathfrak{I}_{h,H}^k v$ is constructed in such a way that it coincides in $k+1$ points on each edge and in $\frac{1}{2}(k+1)(k+2)$ points on each triangular face of the elements.

Remark 2.22 In 2D, we can alternatively follow the idea from [175] and choose a different interpolation operator for $k \geq 2$ on the boundary of the polygonal elements. The introduced points $\mathbf{z}_{E,i}$ from Sect. 2.3.1 can be used for the pointwise interpolation. For $v \in H^2(\Omega)$, this yields

$$\mathfrak{I}_{h,H}^k v = \sum_{\mathbf{z} \in \mathscr{N}_h} v_{\mathbf{z}} \psi_{\mathbf{z}} + \sum_{E \in \mathscr{E}_h} \sum_{i=2}^{k} v_{E,i} \psi_{E,i} \,,$$

where the coefficients are given as

$$v_{\mathbf{z}} = v(\mathbf{z}) \quad \text{for } \mathbf{z} \in \mathscr{N}_h$$

and

$$v_{E,i} = v(\mathbf{z}_{E,i}) - \sum_{j=0}^{i-1} v_{E,j} \psi_{E,j}(\mathbf{z}_{E,j}) \quad \text{for } E \in \mathscr{E}_h,\ i = 2, \ldots, k \,.$$

Next, we consider the definition of the interpolation operator into the space of element bubble functions, namely

$$\mathfrak{I}_{h,B}^k : H^2(K) \to V_{h,B}^k\big|_K \subset H_0^1(K) \,.$$

Therefore, let

$$\Psi_{h,B}^k\big|_K = \{\psi_{K,i} : i = 1, \dots, n(k)\} \quad \text{and} \quad \{p_{K,i} = -\Delta\psi_{K,i} : i = 1, \dots, n(k)\} \tag{2.16}$$

be the basis of $V_{h,B}^k\big|_K$ and the corresponding basis of $\mathscr{P}^{k-2}(K)$, respectively, where $n(k) = \dim V_{h,B}^k\big|_K$ is the number of basis functions. Compare the former definition (2.10)–(2.11) in 2D and the construction (2.15) in 3D. For $v \in H^2(K)$, we have

$$\mathfrak{I}_{h,B}^k v = \sum_{i=1}^{n(k)} v_{K,i}\psi_{K,i} \in V_{h,B}^k\big|_K ,$$

where the coefficients $v_{K,i}$ are defined such that $\mathfrak{I}_{h,B}^k v$ is the orthogonal projection of $v - \mathfrak{I}_{h,H}^k v$ into $V_{h,B}^k\big|_K$ with respect to the weighted inner product

$$(u, v)_{hH^1(K)} = (u, v)_{L_2(K)} + h_K^2(\nabla u, \nabla v)_{L_2(K)} . \tag{2.17}$$

Thus, $\mathfrak{I}_{h,B}^k v$ is uniquely defined by

$$\left(\mathfrak{I}_{h,B}^k v, w\right)_{hH^1(K)} = \left(v - \mathfrak{I}_{h,H}^k v, w\right)_{hH^1(K)} \quad \forall w \in V_{h,B}^k\big|_K . \tag{2.18}$$

The properties of the orthogonal projection yield

$$\|\mathfrak{I}_{h,B}^k v\|_{hH^1(K)} \le \|v - \mathfrak{I}_{h,H}^k v\|_{hH^1(K)} , \tag{2.19}$$

where the weighted norm is given as $\|\cdot\|_{hH^1(K)}^2 = (\cdot,\cdot)_{hH^1(K)}$. If $h_K = 1$ the weighted inner product and the weighted norm coincide with the usual ones in $H^1(K)$, which are denoted by $(\cdot,\cdot)_{H^1(K)}$ and $\|\cdot\|_{H^1(K)}$, respectively.

In the following, we investigate the properties of the interpolation operators in more details. For this purpose, let $\mathscr{K}_h$ be a regular polytopal mesh.

Lemma 2.23 *The restrictions of the interpolation operators $\mathfrak{I}_{h,H}^k$ and $\mathfrak{I}_h^k$ onto an element $K \in \mathscr{K}_h$ satisfy*

$$\mathfrak{I}_{h,H}^k\, p = p \quad \textit{for } p \in \mathscr{P}^k(K) \textit{ with } \Delta p = 0 \textit{ in } K ,$$

and

$$\mathfrak{I}_h^k\, p = p \quad \textit{for } p \in \mathscr{P}^k(K) .$$

Proof Let $p \in \mathscr{P}^k(K)$ with $\Delta p = 0$. According to the definition, $\mathfrak{I}^k_{h,H}\, p$ is given as a classical, nodal interpolation into the space $\mathscr{P}^k_{\mathrm{pw}}(\partial K)$ on the boundary of the element K. Since $p \in \mathscr{P}^k_{\mathrm{pw}}(\partial K)$ and polynomials are preserved by the classical interpolation operators, p and $\mathfrak{I}^k_{h,H}\, p$ are identical on the boundary of the element K. Furthermore, both functions satisfy the Laplace equation inside K. Thus, the unique solvability of the Dirichlet problem for the Laplace equation yields $\mathfrak{I}^k_{h,H}\, p = p$, the first statement of the lemma.

Next, let $p \in \mathscr{P}^k(K)$ and therefore $-\Delta p \in \mathscr{P}^{k-2}(K)$. Since the polynomials $p_{K,i}$ form a basis of $\mathscr{P}^{k-2}(K)$, see (2.16), there are unique coefficients $\beta_{K,i} \in \mathbb{R}$ such that

$$-\Delta p = \sum_{i=1}^{n(k)} \beta_{K,i}\, p_{K,i} \ .$$

Furthermore, we define

$$\widetilde{p} = \mathfrak{I}^k_{h,H}\, p + \sum_{i=1}^{n(k)} \beta_{K,i}\, \psi_{K,i} \ . \tag{2.20}$$

We observe that p as well as $\widetilde{p}$ satisfy the boundary value problem

$$\begin{aligned} -\Delta u &= \sum_{i=1}^{n(k)} \beta_{K,i}\, p_{K,i} \quad \text{in } K \ , \\ u &= p \quad \text{on } \partial K \ , \end{aligned}$$

at least in the weak sense, due to construction. Because of the unique solvability of this problem, we conclude that $p = \widetilde{p}$. By (2.20), we obtain

$$p - \mathfrak{I}^k_{h,H}\, p = \sum_{i=1}^{n(k)} \beta_{K,i}\, \psi_{K,i} \in V^k_{h,B}\big|_K \ .$$

Since $\mathfrak{I}^k_{h,B}\, p$ is defined as orthogonal projection of $p - \mathfrak{I}^k_{h,H}\, p$ into $V^k_{h,B}\big|_K$, it is $\mathfrak{I}^k_{h,B}\, p = p - \mathfrak{I}^k_{h,H}\, p$ and the second statement of the lemma follows. □

A consequence of this lemma is that

$$\mathscr{P}^k(K) \subset V^k_h\big|_K \ ,$$

i.e., the space of polynomials of degree k is locally embedded in the approximation space over each element. Obviously, the element basis functions are essential to capture the non-harmonic polynomials.

Lemma 2.24 *The restrictions of the interpolation operators $\mathfrak{I}_{h,H}^k$ and $\mathfrak{I}_h^k$ onto an element $K \in \mathscr{K}_h$ of a regular and stable polytopal mesh $\mathscr{K}_h$ with $h_K = 1$ are linear and continuous. Furthermore, there are constants c_1 and c_2, which only depend on the regularity and stability parameters of the mesh, on k and on the dimension d, such that*

$$\|\mathfrak{I}_{h,H}^k v\|_{H^1(K)} \leq c_1 \, \|v\|_{H^2(K)} \quad \textit{and} \quad \|\mathfrak{I}_h^k v\|_{H^1(K)} \leq c_2 \, \|v\|_{H^2(K)}$$

for all $v \in H^2(K)$.

Proof The linearity of the operators is obvious, so we only have to prove the given estimates which also ensure the continuity. Therefore, we make use of an auxiliary discretization $\mathscr{T}_h(K)$ of K into simplicial elements, i.e., into triangles ($d = 2$) and tetrahedra ($d = 3$). In two-dimensions, we connect the nodes on the boundary of K with the point $\mathbf{z}_K$ and in three-dimensions we exploit $\mathscr{T}_0(K)$ from Sect. 2.2.2. Since $\mathscr{K}_h$ is regular and stable, these auxiliary meshes are shape-regular in the sense of Ciarlet [58] according to Lemmata 2.3 and 2.14, respectively. Thus, neighbouring simplices share either a common node, edge or face and the aspect ratio of each simplex is uniformly bounded by some constant $\sigma_{\mathscr{T}}$. Because the auxiliary mesh is regular, we can use classical interpolation operators, see e.g. [58]. Let

$$\mathfrak{I}_{\mathscr{T}} : H^2(K) \to \mathscr{P}_{\mathrm{pw}}^k(\mathscr{T}_h(K))$$

be such a classical operator with

$$\|v - \mathfrak{I}_{\mathscr{T}} v\|_{H^1(K)} \leq C_{\mathscr{T},1} h_{\mathscr{T}} |v|_{H^2(K)} \quad \text{and} \quad \|\mathfrak{I}_{\mathscr{T}} v\|_{H^1(K)} \leq C_{\mathscr{T},2} \, \|v\|_{H^2(K)} \tag{2.21}$$

for $v \in H^2(K)$, where $h_{\mathscr{T}} = \max\{h_T : T \in \mathscr{T}_h(K)\}$ and

$$\mathscr{P}_{\mathrm{pw}}^k(\mathscr{T}_h(K)) = \left\{ p \in C^0(K) : \; p\big|_T \in \mathscr{P}^k(T) \;\; \forall T \in \mathscr{T}_h(K) \right\} .$$

The constants $C_{\mathscr{T},1}$ and $C_{\mathscr{T},2}$ only depend on the approximation order k, the space dimension d as well as on $\sigma_{\mathscr{T}}$ and thus on the regularity and stability parameters of the polytopal mesh $\mathscr{K}_h$.

Next, we prove the continuity of $\mathfrak{I}_{h,H}^k$, i.e. the estimate

$$\|\mathfrak{I}_{h,H}^k v\|_{H^1(K)} \leq c \, \|v\|_{H^2(K)} \quad \text{for } v \in H^2(K) \, .$$

Let $v \in H^2(K)$ be fixed. The interpolation $\mathfrak{I}_{h,H}^k v$ satisfies the boundary value problem

$$\begin{aligned} -\Delta u &= 0 \quad && \text{in } K \, , \\ u &= g_v \quad && \text{on } \partial K \, , \end{aligned}$$

where $g_v = \mathfrak{I}^k_{h,H} v\big|_{\partial K}$ is a piecewise polynomial of degree k on the boundary ∂K. We write $u = u_0 + u_g$ with $u_g = \mathfrak{I}_{\mathscr{T}} v$ and obtain the Galerkin formulation

$$\text{Find } u_0 \in H^1_0(K): \quad (\nabla u_0, \nabla w)_{L_2(K)} = -(\nabla u_g, \nabla w)_{L_2(K)} \quad \forall w \in H^1_0(K) ,$$

which has a unique solution. Testing with $w = u_0$ and applying the Cauchy–Schwarz inequality yield

$$|u_0|^2_{H^1(K)} \leq |(\nabla u_g, \nabla u_0)_{L_2(K)}| \leq |u_g|_{H^1(K)} |u_0|_{H^1(K)} ,$$

and consequently

$$|u_0|_{H^1(K)} \leq \|u_g\|_{H^1(K)} = \|\mathfrak{I}_{\mathscr{T}} v\|_{H^1(K)} .$$

Because of the piecewise smoothness of the boundary of K and since it can be embedded into a square of side length h_K, the Poincaré–Friedrichs inequality reads

$$\|w\|_{L_2(K)} \leq h_K \, |w|_{H^1(K)} \quad \text{for } w \in H^1_0(K) ,$$

see e.g. [38]. By the use of the given estimates and $h_K = 1$, we obtain

$$\begin{aligned}
\|\mathfrak{I}^k_{h,H} v\|_{H^1(K)} &\leq \|u_0\|_{H^1(K)} + \|u_g\|_{H^1(K)} \\
&= \left(\|u_0\|^2_{L_2(K)} + |u_0|^2_{H^1(K)} \right)^{1/2} + \|\mathfrak{I}_{\mathscr{T}} v\|_{H^1(K)} \\
&\leq \sqrt{2} \, |u_0|_{H^1(K)} + \|\mathfrak{I}_{\mathscr{T}} v\|_{H^1(K)} \\
&\leq \left(\sqrt{2} + 1 \right) \|\mathfrak{I}_{\mathscr{T}} v\|_{H^1(K)} \\
&\leq c \, \|v\|_{H^2(K)} .
\end{aligned}$$

Finally, we apply the continuity of $\mathfrak{I}^k_{h,H}$ as well as the property (2.19) of $\mathfrak{I}^k_{h,B}$ with $h_K = 1$ and we get

$$\begin{aligned}
\|\mathfrak{I}^k_h v\|_{H^1(K)} &\leq \|\mathfrak{I}^k_{h,H} v\|_{H^1(K)} + \|\mathfrak{I}^k_{h,B} v\|_{H^1(K)} \\
&\leq \|\mathfrak{I}^k_{h,H} v\|_{H^1(K)} + \|v - \mathfrak{I}^k_{h,H} v\|_{H^1(K)} \\
&\leq \|v\|_{H^1(K)} + 2\|\mathfrak{I}^k_{h,H} v\|_{H^1(K)} \\
&\leq c \, \|v\|_{H^2(K)}
\end{aligned}$$

that concludes the proof. □

Remark 2.25 The stability of the mesh $\mathscr{K}_h$ was only needed to ensure the shape-regularity of the auxiliary mesh, such that classical interpolation results on triangular

and tetrahedral meshes can be exploited. Thus, the stability of $\mathscr{K}_h$ can be relaxed as long as the interpolation estimates (2.21) on the auxiliary mesh are guaranteed. This yields the following variants:

1. In 2D, it is sufficient to assume the regularity of $\mathscr{K}_h$. According to Corollary 2.9, the auxiliary mesh $\mathscr{T}_h(K)$ thus satisfy a maximum angle condition. Under these assumptions the classical Lagrange interpolation operator fulfils the desired estimates (2.21), see [110, 114].
2. In 3D, we may assume the regularity and weak stability of $\mathscr{K}_h$, which ensures a maximum angle condition for the tetrahedral auxiliary mesh $\mathscr{T}_0(K)$, see Lemma 2.18. For $k = 1$, this is sufficient to prove the interpolation estimates (2.21) on $\mathscr{T}_0(K)$, but it is still an open question whether these estimates hold for $k > 1$, see [115].

According to the previous remark, the lemma stays valid even if the edges ($d = 2$) and faces ($d = 3$) of the polytopal mesh degenerate in their size. Thus, the edge length h_E may decreases faster than the element diameter h_K such that the uniform estimate $h_K \leq c_{\mathscr{K}} h_E$ is violated in two- and three-dimensions.

The condition $h_K = 1$ in Lemma 2.24 is not satisfied in general. Thus, we introduce a scaling for the elements $K \in \mathscr{K}_h$ such that

$$\widehat{K} \ni \widehat{\mathbf{x}} \mapsto \mathbf{x} = \mathfrak{F}_K(\widehat{\mathbf{x}}) = h_K \widehat{\mathbf{x}} \in K \,. \tag{2.22}$$

Consequently, $h_{\widehat{K}} = 1$ and we set $\widehat{v} = v \circ \mathfrak{F}_K$. Simple calculations show that for $v \in H^\ell(K)$, $\ell \in \mathbb{N}_0$ it is $\widehat{v} \in H^\ell(\widehat{K})$ and

$$|\widehat{v}|_{H^\ell(\widehat{K})} = h_K^{\ell - d/2} |v|_{H^\ell(K)} \,. \tag{2.23}$$

Additionally, it holds

$$(u, v)_{L_2(K)} = h_K^d (\widehat{u}, \widehat{v})_{L_2(\widehat{K})} \quad \text{and} \quad (\nabla u, \nabla v)_{L_2(K)} = h_K^{d-2} (\widehat{\nabla} \widehat{u}, \widehat{\nabla} \widehat{v})_{L_2(\widehat{K})}$$

for $u, v \in H^1(K)$, where $\widehat{\nabla}$ denotes the gradient with respect to $\widehat{x}$. According to the definition of the weighted inner product, see (2.17), we obtain

$$(u, v)_{hH^1(K)} = h_K^d (\widehat{u}, \widehat{v})_{hH^1(\widehat{K})} \,. \tag{2.24}$$

Lemma 2.26 *The restrictions of the interpolation operators $\mathfrak{I}_{h,H}^k$ and $\mathfrak{I}_h^k$ onto an element $K \in \mathscr{K}_h$ satisfy for $v \in H^2(K)$*

$$\widehat{\mathfrak{I}_{h,H}^k v} = \widehat{\mathfrak{I}_{h,H}^k}\, \widehat{v} \qquad \textit{and} \qquad \widehat{\mathfrak{I}_h^k v} = \widehat{\mathfrak{I}_h^k}\, \widehat{v} \,,$$

where $\widehat{\mathfrak{I}_h^k} = \widehat{\mathfrak{I}_{h,B}^k} + \widehat{\mathfrak{I}_{h,H}^k}$ and $\widehat{\mathfrak{I}_{h,H}^k}$ as well as $\widehat{\mathfrak{I}_{h,B}^k}$ are the interpolation operators with respect to the scaled element $\widehat{K}$.

Proof Due to the construction of $\mathfrak{I}_{h,H}^k$ by pointwise evaluations on the boundary ∂K and the harmonic extension, it is obvious that $\widehat{\mathfrak{I}_{h,H}^k v} = \widehat{\mathfrak{I}_{h,H}^k}\,\widehat{v}$. Therefore, we only have to show $\widehat{\mathfrak{I}_{h,B}^k v} = \widehat{\mathfrak{I}_{h,B}^k}\,\widehat{v}$ with $\widehat{\mathfrak{I}_{h,B}^k} : H^2(\widehat{K}) \to \operatorname{span}\{\psi_{\widehat{K},i}\}$. Here, we explicitly refer to the element basis functions $\psi_{K,i}$ and $\psi_{\widehat{K},i}$, cf. (2.16), in order to emphasize the dependence on K and $\widehat{K}$, respectively. Furthermore, it is sufficient to prove

$$\widehat{\mathfrak{I}_{h,B}^k v} \in \operatorname{span}\{\psi_{\widehat{K},i}\}$$

and

$$(\widehat{\mathfrak{I}_{h,B}^k v}, \varphi)_{H^1(\widehat{K})} = (\widehat{\mathfrak{I}_{h,B}^k}\widehat{v}, \varphi)_{H^1(\widehat{K})} \quad \text{for } \varphi \in \operatorname{span}\{\psi_{\widehat{K},i}\}\,,$$

since for $\varphi = \widehat{\mathfrak{I}_{h,B}^k v} - \widehat{\mathfrak{I}_{h,B}^k}\widehat{v}$, we obtain

$$\|\widehat{\mathfrak{I}_{h,B}^k v} - \widehat{\mathfrak{I}_{h,B}^k}\widehat{v}\|_{H^1(\widehat{K})} = 0 \quad \text{and thus} \quad \widehat{\mathfrak{I}_{h,B}^k v} = \widehat{\mathfrak{I}_{h,B}^k}\widehat{v}\,.$$

Here, we have skipped the range $i = 1, \ldots, n(k)$ for shorter notation. In the definition of the element basis functions $\psi_{K,i}$, see (2.10), we have made no specific choice of the polynomials $p_{K,i}$. In the following, let the polynomials for the functions $\psi_{\widehat{K},i}$ over $\widehat{K}$ be chosen in dependence of $\psi_{K,i}$ as

$$p_{\widehat{K},i} = h_K^2\,\widehat{p}_{K,i}\,.$$

In consequence, we obtain for the scaled element function $\widehat{\psi}_{K,i} = \psi_{K,i} \circ \mathfrak{F}_K$ that

$$-\widehat{\Delta}\widehat{\psi}_{K,i} = h_K^2\,\widehat{p}_{K,i} = p_{\widehat{K},i} = -\widehat{\Delta}\psi_{\widehat{K},i} \quad \text{in } \widehat{K}$$

and $\widehat{\psi}_{K,i} = \psi_{\widehat{K},i}$ on ∂K, where $\widehat{\Delta}$ denotes the Laplace operator with respect to $\widehat{x}$. Due to the unique solvability of the Dirichlet problem for the Laplace equation, we get $\psi_{\widehat{K},i} = \widehat{\psi}_{K,i}$ and thus

$$\widehat{\mathfrak{I}_{h,B}^k v} = \sum_{i=1}^{n(k)} v_{K,i}\,\widehat{\psi}_{K,i} \in \operatorname{span}\{\psi_{\widehat{K},i}\}\,.$$

Next, let $\varphi_{\widehat{K}} \in \operatorname{span}\{\psi_{\widehat{K},i}\}$ and set $\varphi_K = \varphi_{\widehat{K}} \circ \mathfrak{F}_K^{-1} \in \operatorname{span}\{\psi_{K,i}\}$. By the definition of $\mathfrak{I}_{h,B}^k$, we have

$$\left(\mathfrak{I}_{h,B}^k v, \varphi_K\right)_{hH^1(K)} = \left(v - \mathfrak{I}_{h,H}^k v, \varphi_K\right)_{hH^1(K)}\,.$$

Applying (2.24) to both sides of the equation yields

$$\begin{aligned}(\widehat{\mathfrak{I}^k_{h,B}v}, \varphi_{\widehat{K}})_{H^1(\widehat{K})} &= (\widehat{v - \mathfrak{I}^k_{h,H}v}, \varphi_{\widehat{K}})_{H^1(\widehat{K})} \\ &= (\widehat{v} - \widehat{\mathfrak{I}^k_{h,H}\widehat{v}}, \varphi_{\widehat{K}})_{H^1(\widehat{K})} \\ &= (\widehat{\mathfrak{I}^k_{h,B}\widehat{v}}, \varphi_{\widehat{K}})_{H^1(\widehat{K})} ,\end{aligned}$$

where the last equality comes from the definition of $\widehat{\mathfrak{I}^k_{h,B}}$ and the fact that the inner products $(\cdot,\cdot)_{hH^1(\widehat{K})}$ and $(\cdot,\cdot)_{H^1(\widehat{K})}$ coincide on the scaled element. Since $\varphi_{\widehat{K}}$ is chosen arbitrarily, this equality concludes the proof. □

Theorem 2.27 *Let $\mathscr{K}_h$ be a regular and stable polytopal mesh of the bounded polytopal domain $\Omega \subset \mathbb{R}^d$, $d = 2, 3$. The interpolation operators $\mathfrak{I}^k_{h,H}$ and $\mathfrak{I}^k_h$ satisfy*

$$\|v - \mathfrak{I}^k_{h,H}v\|_{H^\ell(\Omega)} \le c\, h^{k+1-\ell}\, |v|_{H^{k+1}(\Omega)} \quad \textit{for } v \in H^{k+1}_\Delta(\mathscr{K}_h) ,$$

and

$$\|v - \mathfrak{I}^k_h v\|_{H^\ell(\Omega)} \le c\, h^{k+1-\ell}\, |v|_{H^{k+1}(\Omega)} \quad \textit{for } v \in H^{k+1}(\Omega) ,$$

respectively, where $h = \max\{h_K : K \in \mathscr{K}_h\}$, $\ell = 0, 1$ and the constant c only depends on the mesh parameters, the dimension d and on k.

Proof First, we consider the second estimate and the case $\ell = 1$. Let us start to examine the error over one element $K \in \mathscr{K}_h$. We scale this element in such a way that its diameter becomes one, see (2.22). With the help of (2.23) and Lemma 2.26, we obtain

$$\begin{aligned}\|v - \mathfrak{I}^k_h v\|^2_{H^1(K)} &= \|v - \mathfrak{I}^k_h v\|^2_{L_2(K)} + |v - \mathfrak{I}^k_h v|^2_{H^1(K)} \\ &\le c h_K^d \|\widehat{v} - \widehat{\mathfrak{I}}^k_h\widehat{v}\|^2_{L_2(\widehat{K})} + c h_K^{d-2} |\widehat{v} - \widehat{\mathfrak{I}}^k_h\widehat{v}|^2_{H^1(\widehat{K})} \\ &\le c h_K^{d-2} \|\widehat{v} - \widehat{\mathfrak{I}}^k_h\widehat{v}\|^2_{H^1(\widehat{K})}\end{aligned}$$

since $h_K \le 1$. Let $\widehat{p} \in \mathscr{P}^k(\widehat{K})$ be the polynomial of the Bramble–Hilbert Lemma for star-shaped domains, which closely approximates $\widehat{v}$, see [40]. It satisfies

$$|\widehat{v} - \widehat{p}|_{H^\ell(\widehat{K})} \le C\, h_{\widehat{K}}^{k+1-\ell}\, |\widehat{v}|_{H^{k+1}(\widehat{K})} \quad \text{for } \ell = 0, 1, \ldots, k+1 \tag{2.25}$$

with a constant C that only depends on $\sigma_{\mathscr{K}}$, d and k. Due to the scaling $h_{\widehat{K}} = 1$ and by the application of Lemmata 2.23 and 2.24, we obtain

$$\begin{aligned} \|\widehat{v} - \widehat{\mathfrak{I}}_h^k \widehat{v}\|_{H^1(\widehat{K})} &\leq \|\widehat{v} - \widehat{p}\|_{H^1(\widehat{K})} + \|\widehat{\mathfrak{I}}_h^k(\widehat{v} - \widehat{p})\|_{H^1(\widehat{K})} \\ &\leq (1+c)\, \|\widehat{v} - \widehat{p}\|_{H^2(\widehat{K})} \\ &\leq (1+c) C\, |\widehat{v}|_{H^{k+1}(\widehat{K})} , \end{aligned} \tag{2.26}$$

where we have used (2.25) in the last step. Comparing the previous estimates and transforming back to the element K yields

$$\|v - \mathfrak{I}_h^k v\|_{H^1(K)}^2 \leq c h_K^{2k} \, |v|_{H^{k+1}(K)}^2 .$$

Finally, we have to sum up this inequality over all elements of the mesh and apply the square root to it. This gives

$$\|v - \mathfrak{I}_h^k v\|_{H^1(\Omega)} \leq c \left(\sum_{K \in \mathscr{K}_h} h_K^{2k} \, |v|_{H^{k+1}(K)}^2 \right)^{1/2} \leq c\, h^k \, |v|_{H^{k+1}(K)} ,$$

and finishes the proof for $\ell = 1$. The case $\ell = 0$ follows by

$$\|v - \mathfrak{I}_h^k v\|_{L_2(K)} = h_K^{d/2} \|\widehat{v} - \widehat{\mathfrak{I}}_h^k \widehat{v}\|_{L_2(\widehat{K})} \leq h_K^{d/2} \|\widehat{v} - \widehat{\mathfrak{I}}_h^k \widehat{v}\|_{H^1(\widehat{K})} ,$$

and the same arguments as above.

The error estimate for $\mathfrak{I}_{h,H}^k$ follows in the same way. The case $k = 1$ is already proven since $\mathfrak{I}_{h,H}^1 = \mathfrak{I}_h^1$, thus let $k \geq 2$. The main difference is in (2.25), where we have to ensure that $\widehat{p}$ is harmonic. In the formulation of the Bramble–Hilbert Lemma in [40], $\widehat{p}$ is chosen as Taylor polynomial of $\widehat{v}$ averaged over the inscribed circle or ball of K given by the regularity of the mesh, cf. Definitions 2.1 and 2.11. Furthermore, the commutativity is proven for the operator of the weak derivative and the operator for the averaged Taylor polynomial for $k \geq 2$. Thus, since $\widehat{v} \in H^2(\widehat{K})$ and $\widehat{\Delta}\widehat{v} = 0$ in the weak sense, we obtain that the averaged Taylor polynomial $\widehat{p}$ is harmonic. □

Remark 2.28 The stability of the mesh $\mathscr{K}_h$ in the previous theorem is used only in order to apply Lemma 2.24. This assumption can be weakened in certain cases, see Remark 2.25. The statement of Theorem 2.27 still holds for $d = 2$ if solely the regularity of the mesh is assumed, and for $d = 3$ with $k = 1$ if the mesh is regular and weakly stable.

2.5 Galerkin Formulation and Convergence Estimates

In the previous sections we have discussed the discretization of the Sobolev space $H^1(\Omega)$ and investigated approximation properties. Thus, we come back to the model problem (2.1) and formulate the finite element method with the use of the introduced arbitrary order basis functions. Therefore, we consider in the following a bounded polygonal or polyhedral domain $\Omega \subset \mathbb{R}^d$, $d = 2, 3$ which is meshed by a regular polytopal mesh $\mathscr{K}_h$. In the three-dimensional case $d = 3$, we restrict ourselves to polyhedral elements with triangular faces as discussed in Sect. 2.3.4 and postpone the general case for later considerations.

In the case of inhomogeneous Dirichlet data g_D, we extend this boundary data into the interior of the domain. The extension is denoted by g_D again, and we assume that it can be chosen such that $g_D \in V_h^k$. Let

$$V_{h,D}^k = V_h^k \cap H_D^1(\Omega) \quad \text{with} \quad H_D^1(\Omega) = \{v \in H^1(\Omega) : v|_{\Gamma_D} = 0\} .$$

The Galerkin formulation for the model problem (2.1) reads:

$$\begin{aligned} &\text{Find } u \in g_D + H_D^1(\Omega) : \\ &b(u, v) = (f, v)_{L_2(\Omega)} + (g_N, v)_{L_2(\Gamma_N)} \quad \forall v \in H_D^1(\Omega) , \end{aligned} \tag{2.27}$$

and the corresponding discrete Galerkin formulation:

$$\begin{aligned} &\text{Find } u_h \in g_D + V_{h,D}^k : \\ &b(u_h, v_h) = (f, v_h)_{L_2(\Omega)} + (g_N, v_h)_{L_2(\Gamma_N)} \quad \forall v_h \in V_{h,D}^k , \end{aligned} \tag{2.28}$$

where

$$b(u_h, v_h) = (a \nabla u_h, \nabla v_h)_{L_2(\Omega)}$$

is the well known bilinear form for the diffusion problem. Due to the boundedness of the diffusion coefficient, the bilinear form $b(\cdot, \cdot)$ is bounded and elliptic on $H_D^1(\Omega)$. Because of the conforming approximation space $V_D^k \subset H_D^1(\Omega)$, the Galerkin as well as the discrete Galerkin formulation above admit a unique solution according to the Lax–Milgram Lemma. Céa's Lemma yields

$$\|u - u_h\|_{H^1(\Omega)} \leq c \min_{v_h \in g_D + V_{h,D}^k} \|u - v_h\|_{H^1(\Omega)} .$$

This quasi-best approximation gives rise to error estimates for the finite element formulation. The minimum on the right hand side can be estimated from above by setting $v_h = \mathfrak{I}_h^k u$. Thus, the interpolation estimates derived in Sect. 2.4 turn over to the finite element approximation. By the use of the interpolation properties given

in Theorem 2.27, we obtain the next result. Since the mesh assumptions are mainly needed in order to apply the interpolation error estimates, these assumptions can be relaxed in the following theorems in certain situations, see Remark 2.28.

Theorem 2.29 *Let $\mathscr{K}_h$ be a regular and stable polytopal mesh of the bounded domain $\Omega \subset \mathbb{R}^d$. The solution $u_h \in V_h^k$ of the Galerkin formulation from above satisfies*

$$\|u - u_h\|_{H^1(\Omega)} \leq c\, h^k\, |u|_{H^{k+1}(\Omega)} \quad \text{for } u \in H^{k+1}(\Omega)\,,$$

where $h = \max\{h_K : K \in \mathscr{K}_h\}$ and the constant c only depends on the mesh parameters, the dimension d and on k.

If we assume more regularity for the model problem, the Aubin–Nitsche trick together with Theorem 2.29 can be used to prove an error estimate in the L_2-norm, see, e.g., [40].

Theorem 2.30 *Let $\mathscr{K}_h$ be a regular and stable polytopal mesh of the bounded domain $\Omega \subset \mathbb{R}^d$ and let there be, for any $g \in L_2(\Omega)$, a unique solution of*

$$\text{Find } w \in H_D^1(\Omega): \quad b(v, w) = (g, v)_{L_2(\Omega)} \quad \forall v \in H_D^1(\Omega)\,,$$

with $w \in H^2(\Omega)$ such that

$$|w|_{H^2(\Omega)} \leq C\, \|g\|_{L_2(\Omega)}\,.$$

The solution $u_h \in V_h^k$ of the Galerkin formulation from above satisfies

$$\|u - u_h\|_{L_2(\Omega)} \leq c\, h^{k+1}\, |u|_{H^{k+1}(\Omega)} \quad \text{for } u \in H^{k+1}(\Omega)\,,$$

where the constant c only depends on the mesh parameters, the dimension d and on k.

Proof Since $u - u_h \in H_D^1(\Omega) \subset L_2(\Omega)$, there is a unique $w \in H^2(\Omega)$ such that

$$b(v, w) = (u - u_h, v)_{L_2(\Omega)} \quad \text{for } v \in H_D^1(\Omega)$$

with

$$|w|_{H^2(\Omega)} \leq C\, \|u - u_h\|_{L_2(\Omega)}\,. \tag{2.29}$$

The Galerkin orthogonality

$$b(u - u_h, v_h) = 0 \quad \text{for } v_h \in V_{h,D}^k \subset H_D^1(\Omega)$$

and the continuity of the bilinear form yield for $\mathfrak{I}_h^1 w \in V_{h,D}^k$

$$\begin{aligned}\|u - u_h\|_{L_2(\Omega)}^2 &= (u - u_h, u - u_h)_{L_2(\Omega)} = b(u - u_h, w) \\ &= b(u - u_h, w - \mathfrak{I}_h^1 w) \le c \, \|u - u_h\|_{H^1(\Omega)} \|w - \mathfrak{I}_h^1 w\|_{H^1(\Omega)} \, .\end{aligned}$$

The first term on the right hand side is estimated using Theorem 2.29 and the second by the use of Theorem 2.27. This yields

$$\|u - u_h\|_{L_2(\Omega)}^2 \le c h^{k+1} \, |u|_{H^{k+1}(\Omega)} |w|_{H^2(\Omega)} \, .$$

Applying (2.29) and dividing by $\|u - u_h\|_{L_2(\Omega)}$ gives the desired estimate. □

If the boundary value problem (2.1) has vanishing right hand side, i.e. $f = 0$, and thus the solution satisfies $u \in H_\Delta^1(\mathscr{K}_h)$, we can seek the approximation u_h directly in the subspace $V_{h,H}^k = \operatorname{span} \Psi_{h,H}^k \subset V_h^k$. Consequently, we obtain a reduced Galerkin formulation. The same arguments as above yield optimal rates of convergence, when the interpolation operator $\mathfrak{I}_{h,H}^k$ is used instead of $\mathfrak{I}_h^k$.

Theorem 2.31 *Under the same assumptions as in Theorems 2.29 and 2.30, the solution $u_h \in V_{h,H}^k$ of the reduced Galerkin formulation with $f = 0$ satisfies*

$$\|u - u_h\|_{H^\ell(\Omega)} \le c \, h^{k+1-\ell} \, |u|_{H^{k+1}(\Omega)} \quad \text{for } u \in H_\Delta^{k+1}(\mathscr{K}_h) \, ,$$

where $\ell = 0, 1$ and the constant c only depends on the mesh parameters, the dimension d and on k as well as on ℓ.

Remark 2.32 The stability of the mesh $\mathscr{K}_h$ in the previous theorems can be weakened, cf. Remark 2.25. The statements still hold for $d = 2$ if solely the regularity of the mesh is assumed, and for $d = 3$ with $k = 1$ if the mesh is regular and weakly stable.

In the realization of the discrete Galerkin formulation (2.28), we have to address the evaluation of the bilinear form applied to ansatz functions. Since the diffusion coefficient is assumed to be constant on each element such that $a(\cdot) = a_K \in \mathbb{R}$ on K, for $K \in \mathscr{K}_h$, we have

$$b(\psi, \varphi) = (a \nabla \psi, \nabla \varphi)_{L_2(\Omega)} = \sum_{K \in \mathscr{K}_h} a_K (\nabla \psi, \nabla \varphi)_{L_2(K)} \quad \text{for } \psi, \varphi \in \Psi_h^k \, .$$

We remember that the basis $\Psi_h^k = \Psi_{h,H}^k \cup \Psi_{h,B}^k$ consists of piecewise harmonic functions and element basis functions which vanish on the element boundaries. According to (2.13), it holds

$$b(\psi, \varphi) = 0 \quad \text{for } \psi \in \Psi_{h,H}^k, \, \varphi \in \Psi_{h,B}^k \, , \tag{2.30}$$

and thus the discrete Galerkin formulation (2.28) decouples. If we split the unknown function into

$$u_h = u_{h,H} + u_{h,B} \quad \text{with} \quad u_{h,H} \in V_{h,H}^k \quad \text{and} \quad u_{h,B} \in V_{h,B}^k ,$$

and take $g_D \in V_{h,H}^k$, we obtain with $V_{h,H,D}^k = V_{h,H}^k \cap H_D^1(\Omega)$

$$\begin{aligned} &\text{Find } u_{h,H} \in g_D + V_{h,H,D}^k : \\ &b(u_{h,H}, v_h) = (f, v_h)_{L_2(\Omega)} + (g_N, v_h)_{L_2(\Gamma_N)} \quad \forall v_h \in V_{h,H,D}^k , \end{aligned} \tag{2.31}$$

and

$$\text{Find } u_{h,B} \in V_{h,B}^k : \quad b(u_{h,B}, v_h) = (f, v_h)_{L_2(\Omega)} \quad \forall v_h \in V_{h,B}^k . \tag{2.32}$$

The problem (2.31) turns into a global system of linear equations with a symmetric and positive definite matrix. Since the support of each element basis function lies inside a single element, a closer look at (2.32) shows that the equation further decouples. The element contributions $u_{h,B}\big|_K \in H_0^1(K)$, $K \in \mathscr{K}_h$ are given as solution of

$$(\nabla u_{h,B}\big|_K, \nabla v_h)_{L_2(K)} = (f/a_K, v_h)_{L_2(K)} \quad \forall v_h \in V_{h,B}^k\big|_K$$

for each element $K \in \mathscr{K}_h$. Thus, $u_{h,B}\big|_K$ is locally the orthogonal projection of f/a_K into $V_{h,B}^k\big|_K = \operatorname{span} \Psi_{h,B}^k\big|_K$ the space of element bubble functions with respect to the scaler product $(\nabla\cdot, \nabla\cdot)_{L_2(K)}$. Furthermore, $u_{h,B}$ is separated from the global problem and can be computed via these local projections.

In Theorem 2.31, we already observed that in the case of a vanishing source term, i.e. $f = 0$, it is sufficient to seek the approximation $u_h \in V_h^k$ in the subspace $V_{h,H}^k$. This observation is confirmed by the decoupling of the Galerkin formulation. Because of $u_h = u_{h,H} + u_{h,B}$ with $u_{h,H} \in V_{h,H}^k$, and since the part $u_{h,B} \in V_{h,B}^k$ is uniquely defined by (2.32), we get $u_{h,B} = 0$ for $f = 0$ and thus $u_h = u_{h,H}$.

Furthermore, the property (2.30) and, consequently, the decoupling of the system is very practical from the computational point of view. The global system of linear equations reduces to a system which only involves the degrees of freedom corresponding to nodal and edge basis functions. The unknowns for the element basis functions can be computed independently element-by-element in a preprocessing step. Thus, there is no need for static condensation that is often used in high-order methods to eliminate the element-local degrees of freedom.

The decoupling is also an advantage over the virtual element method in [25]. This method has the same number of unknowns, but the system matrix does not decouple. Thus, a larger system of linear equations has to be solved. Another advantage of the presented strategy in this context is that the approximation u_h can be evaluated,

or at least be approximated, in every point inside the domain with the help of the representation formula (4.3), see next section. The virtual element method, however, needs some postprocessing for the evaluation in an arbitrary point.

Remark 2.33 In the construction of the approximation space V_h^k, we have used the same order k over all edges and elements. However, these Trefftz-like basis functions can be used directly with variable order. There is no difficulty which has to be addressed. This flexibility is advantageous in hp-adaptivity, see [63].

Remark 2.34 More details on the computational realization as well as on the local treatment of the implicitly defined basis functions can be found in Chap. 4 and in particular in Sect. 4.5.

In the case of a continuously varying diffusion coefficient in the model problem (2.1), it is possible to approximate the coefficient a by a piecewise constant function a_h. To analyse the impact of this approximation, the first Strang Lemma [162] is used. Replacing the exact material coefficient in the bilinear form $b(\cdot,\cdot)$ by an approximated one can be seen as an approximation $b_h(\cdot,\cdot)$ of the bilinear form. Let the approximation a_h of a sufficiently regular diffusion coefficient satisfy

$$0 < a_{\min} \leq a_h(\mathbf{x}) \leq a_{\max} \quad \text{for } \mathbf{x} \in \Omega \text{ and } h > 0\,, \tag{2.33}$$

and $a_h(\mathbf{x}) = a_K \in \mathbb{R}$ for $\mathbf{x} \in K$ and $K \in \mathscr{K}_h$. Therefore, the bilinear form $b_h(\cdot,\cdot)$ is uniformly elliptic as well as bounded on V_h^k for $h > 0$, and the variational formulation has a unique solution. The Strang Lemma taken from [58] gives the error estimate

$$\|u - u_h\|_{H^1(\Omega)} \leq c \inf_{v_h \in V_h^k} \left\{ \|u - v_h\|_{H^1(\Omega)} + \sup_{w_h \in V_h^k} \frac{|b(v_h, w_h) - b_h(v_h, w_h)|}{\|w_h\|_{H^1(\Omega)}} \right\}\,,$$

for the Galerkin approximation. Obviously, the error in the finite element method is estimated by two terms. One which gives the quasi-best approximation error and one which measures the error coming from the inexact bilinear form. The latter one can be written and estimated in the form

$$\sup_{w_h \in V_h^k} \frac{|((a - a_h)\nabla v_h, \nabla w_h)|}{\|w_h\|_{H^1(\Omega)}} \leq \sup_{w_h \in V_h^k} \sum_{K \in \mathscr{K}_h} \|a - a_h\|_{L_\infty(K)} \frac{|(\nabla v_h, \nabla w_h)_K|}{\|w_h\|_{H^1(\Omega)}}\,.$$

If the constant values a_K are chosen as averaged Tayler polynomials of order zero over the inscribed circle and ball of Definitions 2.1 and 2.11, respectively, we have $\|a - a_h\|_{L_\infty(K)} \leq c h_K \|a\|_{W^1_\infty(K)}$, see [40], and we obtain after some arguments

$$\sup_{w_h \in V_h^k} \frac{|b(v_h, w_h) - b_h(v_h, w_h)|}{\|w_h\|_{H^1(\Omega)}} \leq c\, h\, \|a\|_{W^1_\infty(\Omega)} \|v_h\|_{H^1(\Omega)}\,.$$

Choosing $v_h = \mathfrak{I}_h^k u$ in the Strang estimate and applying Theorem 2.27 as well as Lemma 2.24 for the interpolation operator yields

$$\|u - u_h\|_{H^1(\Omega)} \leq c\, h^k\, |u|_{H^{k+1}(\Omega)} + c\, h\, \|a\|_{W^1_\infty(\Omega)} \|u\|_{H^2(\Omega)} \quad \text{for } u \in H^{k+1}(\Omega)\,.$$

For high-order methods with $k > 1$, the convergence of the finite element error is dominated by the second term, which comes from the piecewise constant approximation of the diffusion coefficient.

In order to achieve the desired convergence rates, it is necessary to approximate the diffusion coefficient more accurately. For a sufficient regular coefficient a, one can use its interpolation $\mathfrak{I}_h^{k-1} a$, for example. For a more detailed discussion and for implementation details, see [146]. The ideas given there can be generalized to $k > 2$ directly.

2.6 Numerical Examples

Finally, the theoretical results are verified by some computational experiments. Theorems 2.29 and 2.30 are illustrated on a model problem. The BEM-based FEM is applied on a sequence of uniformly refined polygonal meshes. In each step of the refinement the boundary-value problem

$$-\Delta u = f \quad \text{in } \Omega = (0,1)^2\,, \qquad u = 0 \quad \text{on } \Gamma \tag{2.34}$$

is solved, where f is chosen such that $u(\mathbf{x}) = \sin(\pi x_1)\sin(\pi x_2)$ is the unique solution. The initial mesh and some refinements are shown in Fig. 2.12. The successively refined meshes are obtained by dividing each polygonal element as described in Sect. 2.2.3. The Galerkin error $\|u - u_h\|_{H^\ell(\Omega)}$ is computed for the H^1-norm ($\ell = 1$) and the L_2-norm ($\ell = 0$). In Fig. 2.13, the relative errors are plotted with respect to the mesh size $h = \max\{h_K : K \in \mathscr{K}_h\}$ on a logarithmic scale. The slopes of the curves reflect the theoretical rates of convergence for the approximation orders $k = 1, 2, 3$.

Next, we consider the model problem

$$-\Delta u = 0 \quad \text{in } \Omega = (0,1)^2\,, \qquad u = g_D \quad \text{on } \Gamma\,, \tag{2.35}$$

where g_D is chosen such that $u(\mathbf{x}) = \exp(2\pi(x_1 - 0.3))\cos(2\pi(x_2 - 0.3))$ is the unique solution. According to Theorem 2.31, it is sufficient to seek the approximation u_h in the space $V_{h,H}^k$ containing only piecewise weakly harmonic functions. Therefore, the number of degrees of freedom is reduced in the computations. We solve the reduced Galerkin formulation on a sequence of meshes produced by the Matlab tool PolyMesher, see [167], and compute the Galerkin errors as in the previous experiment. Some of the meshes are visualized in Fig. 2.14 and the relative errors are plotted with respect to the mesh size h in Fig. 2.15. The theoretical orders of convergence are achieved by the computations for $k = 1, 2, 3$.

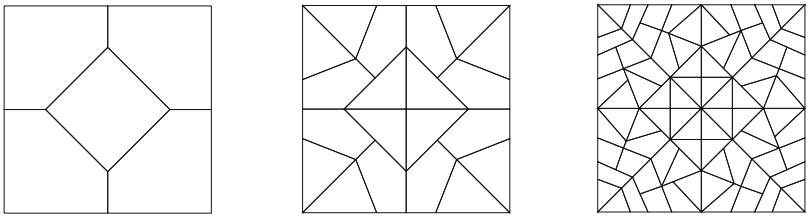

Fig. 2.12 Initial mesh (left), refined mesh after two steps (middle), refined mesh after four steps (right)

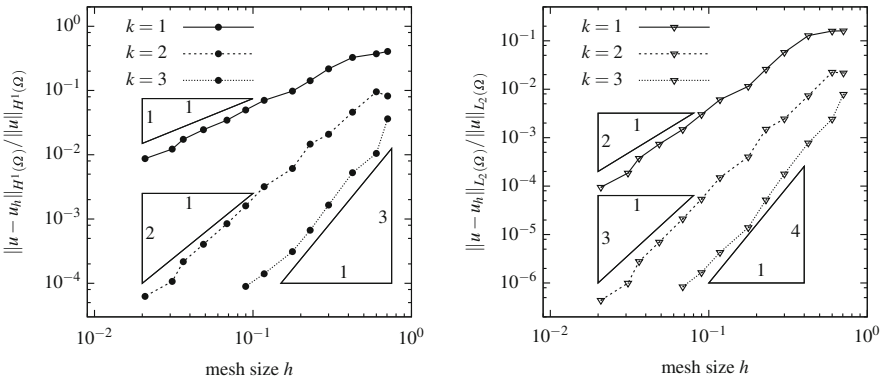

Fig. 2.13 Relative error in H^1-norm (left) and L_2-norm (right) with respect to the mesh size h for problem (2.34) with $u_h \in V_h^k$ on meshes depicted in Fig. 2.12

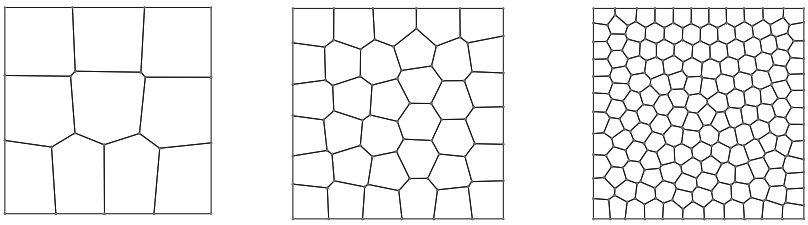

Fig. 2.14 First (left), fourth (middle) and sixth mesh (right) in uniform sequence generated by PolyMesher

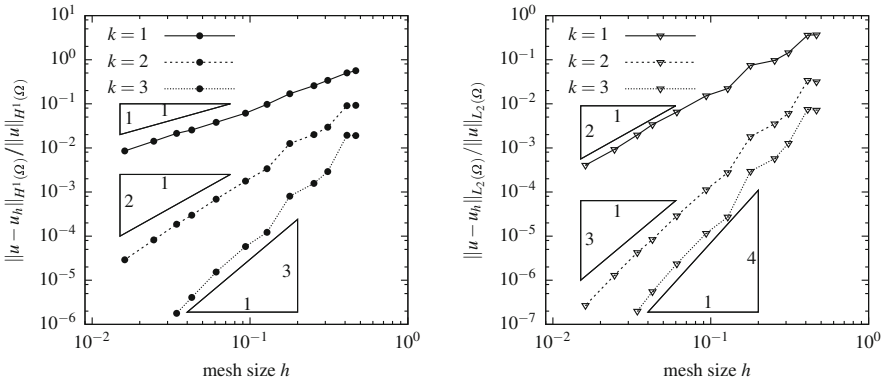

Fig. 2.15 Relative error in H^1-norm (left) and L_2-norm (right) with respect to the mesh size h for problem (2.35) with $u_h \in V^k_{h,H}$ on meshes depicted in Fig. 2.14

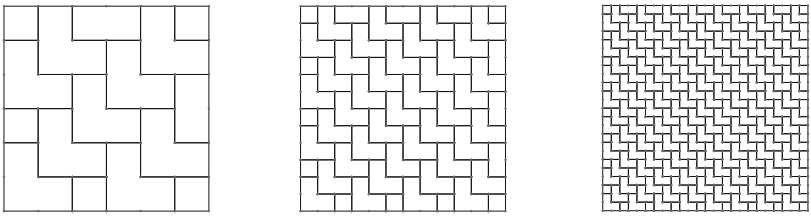

Fig. 2.16 Second (left), third (middle) and fourth mesh (right) in uniform sequence consisting of L-shaped elements and rectangles only

To demonstrate the applicability of the BEM-based FEM on polygonal meshes with non-convex elements, we consider the previous example for the Laplace problem once more. The approach is applied to a sequence of meshes with decreasing mesh size h consisting of L-shaped elements and rectangles only, see Fig. 2.16. On each mesh, the relative error (err) measured in $L_2(\Omega)$ and the numerical order of convergence (noc) are computed, i.e.

$$\text{err} = \frac{\|u-u_h\|_{L_2(\Omega)}}{\|u\|_{L_2(\Omega)}} \qquad \text{and} \qquad \text{noc} = \frac{\log(\|u-u_{2h}\|_{L_2(\Omega)}) - \log(\|u-u_h\|_{L_2(\Omega)})}{\log 2}\,.$$

In Table 2.1, the computed values are given together with the degrees of freedom in the trial space $V^k_{h,H,D} = V^k_{h,H} \cap H_D(\Omega)$ for $k = 1, 2, 3$. The results clearly demonstrate the optimal rates of convergence according to Theorem 2.31, where in the finest example for $k = 3$ saturation of accuracy is reached.

Table 2.1 Degrees of freedom (DoF), relative error measured in $L_2(\Omega)$ (err) and numerical order of convergence (noc) for problem (2.35) with $u_h \in V_{h,H}^k$ on meshes depicted in Fig. 2.16

	$k=1$			$k=2$			$k=3$		
h	DoF	err	noc	DoF	err	noc	DoF	err	noc
9.43×10^{-1}	4	3.73×10^{-1}	–	12	3.48×10^{-2}	–	20	7.96×10^{-3}	–
4.71×10^{-1}	25	9.50×10^{-2}	1.97	65	3.50×10^{-3}	3.31	105	4.71×10^{-4}	4.08
2.36×10^{-1}	121	2.57×10^{-2}	1.88	297	3.90×10^{-4}	3.17	473	2.81×10^{-5}	4.07
1.18×10^{-1}	529	6.34×10^{-3}	2.02	1265	4.67×10^{-5}	3.06	2001	1.71×10^{-6}	4.04
5.89×10^{-2}	2209	1.58×10^{-3}	2.01	5217	5.72×10^{-6}	3.03	8225	1.05×10^{-7}	4.03
2.95×10^{-2}	9025	3.94×10^{-4}	2.00	21,185	7.07×10^{-7}	3.02	33,345	6.30×10^{-9}	4.05
1.47×10^{-2}	36,481	9.83×10^{-5}	2.00	85,377	8.30×10^{-8}	3.09	134,273	2.89×10^{-10}	4.44
7.37×10^{-3}	146,689	2.46×10^{-5}	2.00	342,785	1.03×10^{-8}	3.01	538,881	2.77×10^{-10}	–
Theory:			2			3			4

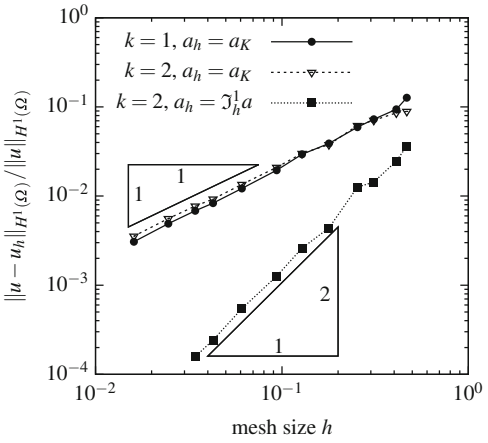

Fig. 2.17 Relative error in H^1-norm with respect to the mesh size h for problem (2.36) with $u_h \in V_h^k$ and different approximations a_h of the diffusion coefficient a on meshes depicted in Fig. 2.14

In order to study the effects of the approximation of the diffusion coefficient we consider the boundary value problem

$$-\operatorname{div}\left(\frac{1}{|\mathbf{x}-\mathbf{x}^*|}\nabla u\right) = 0 \quad \text{in } \Omega = (0,1)^2, \qquad u = g_D \quad \text{on } \Gamma\,, \tag{2.36}$$

where $\mathbf{x}^* = (-0.1, 0.2)^\top$. The Dirichlet boundary data g_D is chosen in such a way that $u(\mathbf{x}) = |\mathbf{x} - \mathbf{x}^*|$ is the exact solution. We apply the approach with the approximation space V_h^k on the uniform sequence generated by the PolyMesher, cf. Fig. 2.14. In the case of a piecewise constant approximation of the diffusion coefficient $a(\mathbf{x}) = |\mathbf{x} - \mathbf{x}^*|^{-1}$, the first order method for $k = 1$ converges with optimal order in the H^1-norm, whereas the second order method for $k = 2$ has a suboptimal convergence rate, see Fig. 2.17. This behaviour has been discussed theoretically in Sect. 2.5, where we observed that the error in the piecewise constant approximation of the diffusion coefficient dominates the convergence process for $k > 1$. Approximating a by $a_h = \mathfrak{I}_h^{k-1} a$, we recover the optimal rates, see Fig. 2.17. For a discussion of the implementation we refer the interested reader to [146].

Finally, a three-dimensional boundary value problem is considered

$$-\operatorname{div}(a\nabla u) = f \quad \text{in } \Omega = (0,1)^3, \qquad u = g_D \quad \text{on } \Gamma\,, \tag{2.37}$$

where $a(\mathbf{x}) = \frac{7}{2} - x_1 - x_2 - x_3$ and f as well as g_D are chosen such that the exact solution is $u(\mathbf{x}) = \cos(\pi x_1)\sin(2\pi x_2)\sin(3\pi \mathbf{x}_3)$. The diffusion coefficient is approximated by a piecewise constant function. The boundary value problem is solved on a uniform sequence of polyhedral meshes, the first one is depicted in

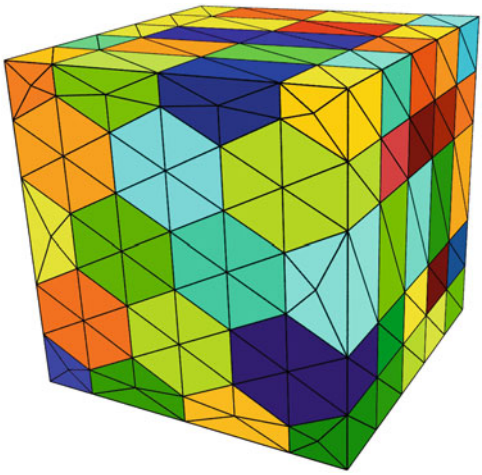

Fig. 2.18 First mesh of unit cube with tessellation of hexahedral bricks and triangular faces

Table 2.2 Degrees of freedom (DoF), relative error measured in the energy norm as well as in the $L_2(\Omega)$-norm with numerical order of convergence (noc) for problem (2.37) with $u_h \in V_h^1$ on meshes with triangulated faces, cf. Fig. 2.18

h	DoF	Energy err	noc	L_2-err	noc
4.23×10^{-1}	152	1.43×10^{0}	–	5.09×10^{-1}	–
2.17×10^{-1}	1176	7.86×10^{-1}	0.90	1.95×10^{-1}	1.44
1.46×10^{-1}	3936	5.40×10^{-1}	0.95	9.61×10^{-2}	1.79
1.10×10^{-1}	9296	4.10×10^{-1}	0.97	5.67×10^{-2}	1.87
8.73×10^{-2}	19,026	3.20×10^{-1}	1.06	3.48×10^{-2}	2.10
7.31×10^{-2}	32,575	2.69×10^{-1}	0.97	2.49×10^{-2}	1.89
6.28×10^{-2}	51,388	2.33×10^{-1}	0.98	1.86×10^{-2}	1.90
5.51×10^{-2}	76,329	2.04×10^{-1}	0.98	1.45×10^{-2}	1.92
4.87×10^{-2}	111,188	1.79×10^{-1}	1.07	1.12×10^{-2}	2.12
Theory:			1		2

Fig. 2.18. The meshes are constructed with the help of hexahedral bricks, where the polygonal faces are triangulated in order to apply the simple generalization for the three-dimensional approximation space in Sect. 2.3.4. The relative errors in the energy norm $\|\cdot\|_b = \sqrt{b(\cdot,\cdot)}$ and the L_2-norm are computed and given in Table 2.2. Furthermore, we give the numerical orders of convergence (noc), cf. (1.7), with respect to these norms. We observe linear convergence in the energy norm and quadratic convergence in the L_2-norm as predicted by the theory.